Discretization effects in the finite element simulation of seismic shear waves in elastic and elastic-plastic media

Kohei Watanabe[1], Federico Pisanò[2], Boris Jeremić[3,4]

[1] Shimizu Corporation, Tokyo, Japan

[2] Delft University of Technology, Delft, The Netherlands

[3] University of California, Davis, California, U.S.A.

[4] Lawrence Berkeley National Laboratory, Berkeley, California, U.S.A.

Corresponding author: B. Jeremić, phone (530) 754-9248. fax (530) 754-7872,

Email: jeremic@ucdavis.edu

Abstract

Presented here is a numerical investigation that (re-)appraises standard rules for space/time discretization in seismic wave propagation analyses. Although the issue is almost off the table of research, situations are often encountered where (established) discretization criteria are not observed, and unsatisfactory results are obtained. In particular, detailed analysis of discretization criteria is developed for wave propagation through both elastic and elastic-plastic materials. The establishment of such criteria is especially important when accurate prediction of high-frequency motion is needed and/or in the presence of markedly non-linear material models.

Current discretization rules for wave problems in solids are critically assessed as a *conditio sine qua non* for improving verification/validation procedures in applied seismology and earthquake engineering. For this purpose, propagation of shear waves through a 1D stack of 3D finite elements have been performed, including the use of wide-band input motions in combination with both linear elastic and non-linear elastic-plastic material models. The blind use of usual rules of thumb is shown to be sometimes debatable, and an effort is made to provide improved discretization criteria. Possible pitfalls of wave simulations are pointed out by showing the dependence of discretization requirements may be requirements on time duration, spatial location, material model and the specific output variable considered.

keywords: wave propagation, seismic, discretization, elastic, elastic-plastic, verification

1 Introduction

The study of wave motion is of utmost importance in many applied sciences, and supports the understanding of transient phenomena in most natural and anthropic dynamic systems. In this field, the case of mechanical waves in solid media plays a major role because of its connection to a number of hazardous events, such as blasts, earthquakes, structural vibrations, etc. (Semblat and Pecker, 2009). In this respect, seismic waves propagating through the earth crust deserve the highest consideration, especially in the light of their destructive potential and socio-economical impact.

In the last decades, mathematicians, geophysicists and engineers devoted massive research efforts to enhance the capability of predicting/mitigating the effects of earthquakes on natural environments and human lives. Depending on the analysis approach adopted, feasible solutions of seismic wave problems can be classified as:

- *Analytical*, i.e. exact mathematical solutions of dynamic boundary value problems. In most cases, these account for idealized/simplified geometries, boundary conditions, etc. (Kolsky, 1963; Graff, 1975; Kausel and Manolis, 2000; Lai and Wilmanski, 2005; Kausel, 2006);

- *Numerical*, i.e. obtained through approximate computational methods and also possible in the presence of inhomogeneous properties, geometrical irregularities, material non-linearities, etc. (Argyris and Mlejnek, 1991; Kramer, 1996; Zienkiewicz et al., 1999).

When linear (elastic) wave problems are considered, either time-domain or frequency-domain solutions may be sought, whereas time-domain approaches are usually needed in the presence of non-linearities (constitutive or geometrical). In this respect, it is worth remarking that most of the interest in seismology, applied geophysics and earthquake engineering is nowadays on non-linear wave phenomena, since they govern (i) the occurrence of instabilities (e.g. soil liquefaction and strain localization (Ishihara, 1996; Zienkiewicz et al., 1999; di Prisco and Wood, 2012) and related catastrophic events in earth crust materials (landslides, avalanches, debris flows, soil sinking, etc.); (ii) the energetic interaction between geomaterials and man-made structures (Wolf, 1985; Gazetas and Mylonakis, 1998; Chopra, 2000; Jeremić et al., 2009; Semblat and Pecker, 2009; Randolph and Gourvenec, 2011; di Prisco and Pisanò, 2011).

It is thus apparent that reliable numerical simulations of seismic motion and earthquake-soil-structure interaction can be only performed by means of high-fidelity computational tools, capable of coping with the remarkable complexities in the aforementioned problems. The accuracy of numerical predictions is affected – at least – by the following four factors:

1. selection of a suitable numerical algorithm for solving the governing equations of motions;

2. constitutive modeling, i.e. the mathematical description of the material behavior;

3. computer implementation of the numerical algorithm and constitutive equations;

4. setup of the computational model, that is, a numerical, discrete representation of physical reality.

Assessing the above four points is the main core of a thorough verification and validation process (Oberkampf et al., 2004; Babuska and Oden, 2004; Roy and Oberkampf, 2011): is the mathematical problem numerically solved to the desired degree of accuracy? Do numerical results reasonably reproduce real world phenomena?

The present work focuses on the fourth item in the list, i.e. on the setup of seismic wave propagation models via the Finite Element (FE) approach[1]. The main issue is on the selection of proper time step and element size. In the context of applied seismology and earthquake engineering, the problem seems to have been solved quite long ago in the form of a few "rules of thumb" for space/time discretization (Lysmer and Kuhlemeyer, 1969; Kuhlemeyer and Lysmer, 1973). Since then, not many works on the subject have been published to the authors' knowledge (Smith, 1975; Bayliss et al., 1985; Bao et al., 1998; De Basabe and Sen, 2007), so that most new papers on seismic wave problems tend to take the aforementioned rules for granted. Furthermore, the relationship between discretization and accuracy in wave problems has been mainly investigated by performing theoretical analyses for numerical attenuation and dispersion, which is doable only for linear problems.

In the light the above premises, the authors aim an up-to-date contribution to the matter, also accounting for the increased importance assumed in recent years by non-linear, elastic-plastic wave problems. For the sake of clarity, the key points of the present work are hereafter summarized:

- only 1D shear wave propagation tests are considered, in order to benefit from the easier (partly analytically supported) interpretation of the numerical outcomes;

- discretization effects are illustrated in both the time and frequency domains, **and then quantified via modern misfit criteria formulated in the full time-frequency domain**;

- since discretization effects depend in general on the numerical algorithm adopted, a widespread finite element approximation scheme has been here adopted;

- the role of constitutive non-linearities is discussed;

[1]The extensive literature on the Finite Difference Method is not mentioned here

– the whole study has been conceived as a numerical "falsification test" for the "rules of thumb" previously mentioned (Lysmer and Kuhlemeyer, 1969; Kuhlemeyer and Lysmer, 1973).

The ultimate goal of this work is to reopen the debate on the accuracy of wave simulations from a verification/validation perspective, and in the presence of constitutive non-linearities. The results reported provide renovated critical insight into, and review of, traditional discretization rules for practical simulation purposes.

2 FE modeling of 1D seismic wave propagation

1D shear wave problems originate from those ideal situations where wave propagation is nearly vertical, with no lateral geometrical/material inhomogeneities. In these conditions, all vertical cross-section can be regarded as symmetry planes and the soil deposit undergoes a "double plane-strain" deformation, with both horizontal direct strains prevented by symmetry (Prevost, 1989; Borja et al., 1999). As a consequence, unknown variables only depend on time and the vertical spatial coordinate (the problem is geometrically one-dimensional), though the stress state is still multi-axial (di Prisco et al., 2012). The initial-boundary value problem under consideration is sketched in Figure 1.

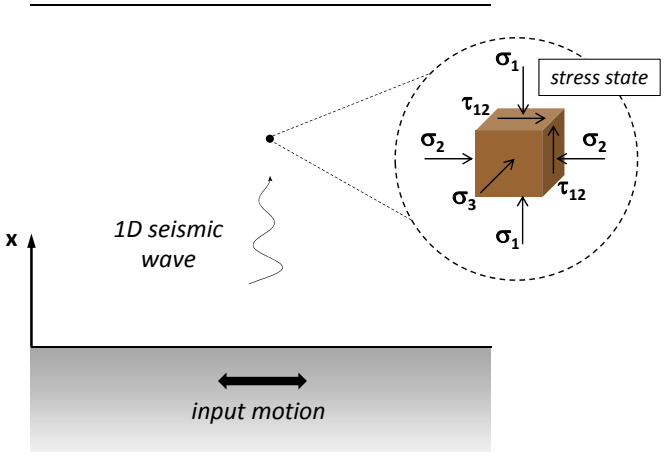

Figure 1: One dimensional (1D) shear wave propagation through a soil layer

Like in general 3D problems, the numerical analysis of 1D seismic wave propagation requires a suitable computational platform for (i) space/time discretization, (ii) material modeling and (iii) simulation under given initial/boundary conditions. The Real ESSI Simulator has been used here for all modeling and simulation.

The Real ESSI Simulator is a software, hardware and documentation system developed specifically for high fidelity, realistic modeling and simulation of earthquake soil structure interaction (ESSI). The Real ESSI program features a number of simple and advanced modeling features. For example, on the finite element side, available are solids elements (8, 20, 27, 8-27 node, dry and saturated bricks), structural elements (trusses, beams, shells), contact elements (frictional slip and gap, dry and saturated), isolator and dissipator elements. On the material modeling side, available are elastic (isotropic, anisotropic, linear and nonlinear) and elastic-plastic models (isotropic, anisotropic hardening). The seismic input can be applied using the Domain Reduction Method (Bielak et al., 2003; Yoshimura et al., 2003). Both sequential and parallel versions (the latter uses the Plastic Domain Decomposition (PDD) method (Jeremić and Jie, 2008) are available. **Recent applications of Real ESSI to seismic problems are documented, for instance, in Jeremić et al. (2008, 2009); Cheng and Jeremić (2009); Taiebat et al. (2010); Jeremić et al. (2013a,b); Tasiopoulou et al. (2015a,b); Orbović et al. (2015).**

2.1 Space discretization and time marching

The essence of the finite element (FE) approximation scheme lies in the way in which the governing field equations are discretized in space and time. A number of options are available (Zienkiewicz and Taylor, 2000), however, the most widespread approach for Solid Dynamics has been here followed in order to draw helpful conclusions for as many users as possible.

The Real ESSI program is based on a standard displacement FE formulation, where displacement components are taken as unknown variables in the numerical approximation (Zienkiewicz and Taylor, 2000). As for space discretization, the 1D FE model has been built by using a stack of properly constrained 3D brick elements – as was previously done, for instance, by Borja et al. (1999). Real ESSI program enables the use of 8-, 20-, 8-27, and 27-node elements, so that a number of options are given in terms of spatial interpolation degree.

The well-known Newmark method has been adopted for time marching (Newmark, 1959). The main feature of the integration algorithm relates to the approximate series expansion for displacement and velocity components, u and $\dot{u}$ respectively:

$$ {}^{n+1}u = {}^{n}u + \Delta t\, {}^{n}\dot{u} + \Delta^2 t \left[\left(\frac{1}{2} - \beta \right) {}^{n}\ddot{u} + \beta\, {}^{n+1}\ddot{u} \right] \tag{1} $$

$$ {}^{n+1}\dot{u} = {}^{n}\dot{u} + \Delta t \left[(1-\gamma)\, {}^{n}\ddot{u} + \gamma\, {}^{n+1}\ddot{u} \right] \tag{2} $$

between two subsequent time-steps n and $n+1$. Importantly, the expansion uses two parameters, β and γ, governing the accuracy and stability properties of the algorithm. While the reader is addressed to Hughes (2012) for an exhaustive mathematical analysis, it is worth reminding that

the algorithm is unconditionally stable as long as:

$$\gamma \geq \frac{1}{2}, \quad \beta = \frac{1}{4}\left(\gamma + \frac{1}{2}\right)^2 \tag{3}$$

$\gamma = 1/2$ is required for second-order accuracy, whereas any γ larger than $1/2$ introduces numerical attenuation (damping). In this study, the pair $\gamma = 0.5$ and $\beta = 0.25$ (no algorithmic/numerical dissipation) have been exclusively considered.

2.2 Material modeling

The Real ESSI program provides a number of material modeling options, ranging from the simple linear-elastic to advanced elastic-plastic constitutive relationships for cyclically loaded soils (Zienkiewicz et al., 1999; di Prisco and Wood, 2012). Hereafter, the material models adopted for wave propagation analyses are briefly described, namely (i) the standard linear elastic material model, (ii) the elastic-plastic von Mises model with linear kinematic hardening (Lemaitre and Chaboche, 1990; Jeremić et al., 1989-2015) and (iii) the bounding surface elastic-plastic model by Pisanò and Jeremić (2014).

2.2.1 Linear elastic model

Discretization issues will be first investigated for fully linear elastic problems. While the main concepts in linear elasticity relevant to wave dynamics can be found in Graff (1975), it is worth reminding the relationship between the shear wave velocity V_s and the two elastic constitutive parameters (Young's modulus E and Poisson's ratio ν):

$$V_s = \sqrt{\frac{E}{2\left(1+\nu\right)\rho}} = \sqrt{\frac{G}{\rho}} \tag{4}$$

where ρ is the soil mass density and $G = E/(2\left(1+\nu\right))$ the elastic shear modulus. As will be stressed in the following, V_s plays a major role in the selection of proper element size and time-step.

2.2.2 Elastic-plastic: von Mises kinematic hardening (VMKH) model

The relationship among discretization, accuracy and material non-linearity will be first explored through an elastic-plastic von Mises constitutive law with linear kinematic hardening, of the same kind described in Lemaitre and Chaboche (1990); Jeremić et al. (1989-2015).

The VMKH model is very well-known in literature and widely employed for cyclically loaded metals; the application to soil dynamics is limited to undrained loading conditions, i.e. when pore water drainage is prevented and soils can be regarded as cohesive materials in the framework

of total stress analysis (Zienkiewicz et al., 1999; Nova, 2012). Although the assumption of linear hardening is not the most accurate for soils[2], it has been here introduced for numerical convenience. In fact, owing to linear hardening, the post-yielding stiffness is constant, not strain-dependent: this implies an unrealistic unbounded strength, but allows to identify the elastic-plastic shear stiffness with no ambiguity. Only four constitutive parameters need to be set:

- two elastic parameters – E and ν – for the pre-yielding elastic response;
- one yielding parameter – k – proportional to the initial size of the cylindrical yield locus in the stress space;
- one hardening parameter – h – governing the post-yielding (elastic-plastic) stiffness.

The results from wave propagation analyses will clearly show the kind of stress-strain response arising from the VMKH formulation.

2.2.3 Elastic-plastic: Pisanò bounding surface (PBS) model

The more sophisticated constitutive relationship recently proposed by Pisanò and Jeremić (2014) has been also used. At variance with the aforementioned VMKH formulation, the Pisanò bounding surface (PBS) model can quite accurately reproduce important aspects of monotonic/cyclic soil behavior (Kramer, 1996; Wood, 2004; Nova, 2012), such as:

1. development of inelastic strains at the very onset of loading. This is properly reproduced by exploiting the concept of "vanishing yield locus";
2. frictional shear strength, i.e. depending on the effective confining pressure;
3. non-linear hardening, implying a continuous transition from small-strain to failure stiffness;
4. coupling between shear and volumetric strains;
5. average stiffness degradation and damping during cyclic shear loading.

A remarkable quality of the PBS constitutive formulation is the low number of input parameters required (only seven), which makes the model particularly suitable for practical use:

- two elastic parameters – E and ν – to characterize the material behavior at vanishing strains;
- one shear strength parameter – M – directly related to the material frictional angle;

[2]Non-linear hardening models should rather be used – see e.g. Borja and Amies (1994); Borja et al. (1999)

– two parameters – k_d and ξ – governing the development of plastic volumetric strains during shearing;

– two hardening parameters – h and m – to be identified on the basis of stiffness degradation and damping cyclic curves.

For the sake of brevity, interested readers are addressed to Pisanò and Jeremić (2014) for details about formulation, performance and calibration. Evidence of the simulated PBS stress-strain response under cyclic loading will be given in the following sections.

2.3 Initial/boundary conditions and input motion

All the FE results hereafter presented have been obtained under the following initial/boundary conditions (Figure 1):

1. the system is initially still (nil initial velocities and accelerations) with an at–rest geostatic stress state (Nova, 2012);

2. a x–displacement time history is imposed at the bottom boundary to reproduce rigid bedrock conditions;

3. the top boundary is unloaded (free surface);

4. the aforementioned "double plane-strain" conditions has been achieved by (i) preventing the y-displacement throughout the whole model, and (ii) imposing master/slave connections to nodes at the same level z (tied nodes).

The last item in the list regards the fulfilment of 1D symmetry requirements and guarantees the brick stack to undergo a "shear beam"–like deformation (Kramer, 1996).

As far as the input displacement is concerned, the Ormsby wavelet (Ryan, 1994) fits the authors' intent:

$$u(t) = A\left[\frac{(\pi f_4)^2}{\pi f_4 - \pi f_3}\mathrm{sinc}^2(\pi f_4 t) - \frac{(\pi f_3)^2}{\pi f_4 - \pi f_3}\mathrm{sinc}^2(\pi f_3 t)\right] - \left[\frac{(\pi f_2)^2}{\pi f_2 - \pi f_1}\mathrm{sinc}^2(\pi f_2 t) - \frac{(\pi f_1)^2}{\pi f_2 - \pi f_1}\mathrm{sinc}^2(\pi f_1 t)\right] \tag{5}$$

where t denotes the physical time and A the signal amplitude, $\mathrm{sinc}(x) = (\sin x)/x$ is the cardinal sine function, f_i $(i = 1, 2, 3, 4)$ stand for the low-cut, low-pass, high-cut and high-pass frequencies, respectively. The meaning of the f_i frequencies can be inferred from Figure 2(b), illustrating the amplitude Fourier spectrum of function (5). In particular, the suitability of the Ormsby wavelet has a twofold motivation:

1. function (5) has a number of sign reversals and will induce several loading/unloading cycles into the soil undergoing wave motion (Figure 2(a));

2. the peculiar flat branch in the amplitude Fourier spectrum (Figure 2(b)) is a very convenient feature for accuracy assessments in the frequency domain (see next section).

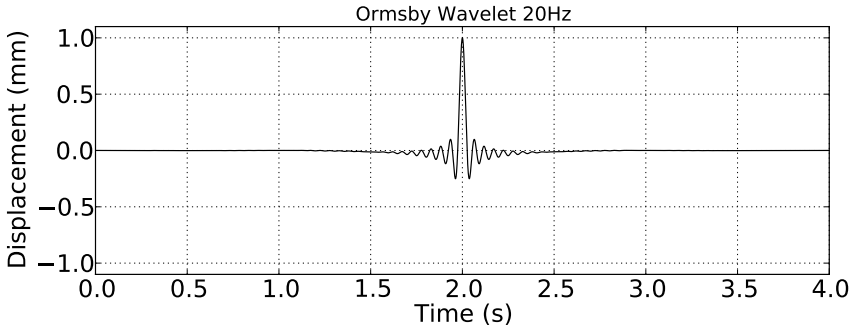

(a) Time history

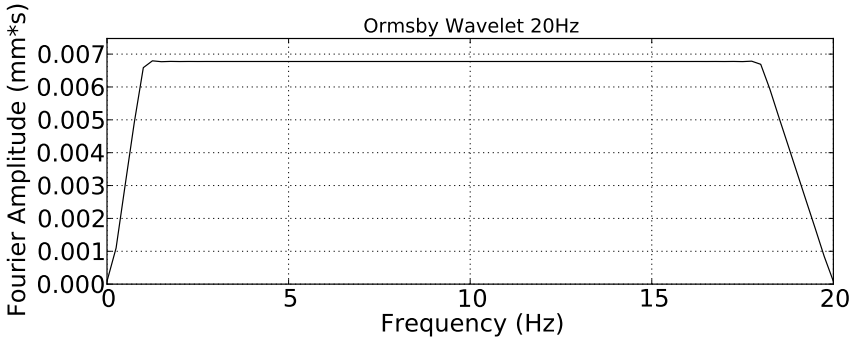

(b) Amplitude of Fourier spectrum

Figure 2: Ormsby wavelet (f_1=0.1 Hz, f_2=1 Hz, f_3=18 Hz, f_4=20 Hz)

The above features of the Ormsby wavelet will allow to explore discretization effects over frequency ranges of choice. In fact, although most seismic energy relates to frequencies lower than 20 Hz, ensuring accuracy at higher frequencies may be relevant when seismic serviceability analyses are to be performed for structures, systems and components (SSCs) related to nuclear power plants and other industrial objects.

2.4 Misfit criteria

The analysis of discretization effects requires objective criteria to quantify the discrepancy (misfit) between different numerical solutions. In numerical seismology, the difference seismogram between the numerical solution and a reliable reference solution is often adopted for this purpose, although it only enables visual/qualitative

observations; simple integral criteria (e.g. root mean square misfit) can provide some quantitative insight, but still with no distinction of amplitude or phase errors.

A significant improvement in this area was introduced by Kristekova et al. (2006), who compared seismograms on the basis of the time-frequency representation (TFR) obtained through continuous wavelet transformation (Holschneider, 1995). The TFR of signal misfit allows to extract the time evolution of the spectral content, and thus to define the following local time-frequency envelope difference:

$$\Delta E\left(t,f\right)=\left|W\left(t,f\right)\right|-\left|W_{REF}\left(t,f\right)\right| \tag{6}$$

and time-frequency phase difference:

$$\Delta P\left(t,f\right)=\left|W_{REF}\left(t,f\right)\right|\frac{\arg\left[W\left(t,f\right)\right]-\arg\left[W_{REF}\left(t,f\right)\right]}{\pi} \tag{7}$$

where $W\left(t,f\right)$ and $W_{REF}\left(t,f\right)$ are the TFR (wavelet transform) of the signal "under evaluation" and the reference seismogram, respectively. As explained by Kristekova et al. (2006), it is also possible to obtain purely time- or frequency-dependent misfit measures by projecting ΔE and ΔP onto one of the two domains. In particular, the following single-values measures for envelope misfit (EM)

$$EM=\sqrt{\frac{\sum_{f}\sum_{t}\left|\Delta E\left(t,f\right)\right|^{2}}{\sum_{f}\sum_{t}\left|W_{REF}\left(t,f\right)\right|^{2}}} \tag{8}$$

and phase misfit (PM)

$$PM=\sqrt{\frac{\sum_{f}\sum_{t}\left|\Delta P\left(t,f\right)\right|^{2}}{\sum_{f}\sum_{t}\left|W_{REF}\left(t,f\right)\right|^{2}}} \tag{9}$$

may be employed to separate amplitude and phase errors when comparing different signal couples. It should be recalled that the envelope function of an oscillating signal is the smooth curve outlining its extremes, and therefore carrying more information than a single amplitude value at given time. While the theoretical background for the above misfit criteria is widely described by Kristekova et al. (2006, 2009), open-source routines for misfit analysis are available at `www.nuquake.eu/ComputerCodes/` (TF-MISFITS package). Discretization effects in wave propagation simulations will be assessed in the following on the basis of EM and PM criteria, as previously done by a number of authors (Pérez-Ruiz et al., 2007; Moczo et al., 2007; Benjemaa et al., 2007; Kaser et al., 2008; Fichtner and Igel, 2008).

3 Linear elastic wave simulations

In this section, the influence of discretization on accuracy is first discussed for fully linear elastic problems. In this context, the insight coming from the well-known analytical solution can be

exploited to critically reconsider standard rules for space/time discretization.

3.1 Standard rules for space/time discretization

The selection of appropriate grid spacing[3] and time-step size is usually based on very simple rules. As for space discretization, Lysmer and Kuhlemeyer (1969) stated that "*the accuracy of the finite element method depends on the ratio obtained by dividing the length of the side of the largest element by the minimum wavelength of elastic waves propagating in the system. For accurate results this ratio should be smaller than 1/12*". Since then, it has been believed that approximately ten nodes per wavelength are appropriate in most cases, whereas fewer than ten nodes are likely to result in undesired numerical attenuation/dispersion. Accordingly, suitable maximum grid spacing is usually determined by considering the minimum relevant wavelength (or highest frequency f_{max}) in the input signal (Jeremić et al., 2009):

$$\Delta x \leq \frac{\lambda_{min}}{10} = \frac{V_s}{10 f_{max}} \tag{10}$$

On the other side, the time-step size also needs to be limited to ensure accuracy and stability (Argyris and Mlejnek, 1991). In principle, the smallest fundamental period of the system should be represented with about ten time-steps – same as for space discretization. However, Δt is often selected on the basis of a different physical argument, i.e. to avoid that a given wave front reaches two consecutive nodes at the same time (this would happen for too large Δt values):

$$\Delta t \leq \frac{\Delta x}{V_s} \tag{11}$$

Condition (11) ensures algorithmic stability in many explicit schemes for hyperbolic differential problems (Quarteroni and Valli, 2008), though it is often regarded as an accuracy criterion for implicit (unconditionally stable) time marching as well (see section 2.1).

3.2 Model parameters

The geometrical/mechanical parameters adopted for elastic wave simulations are here reported. A uniform soil layer has been considered, having thickness H=1 km and made of an elastic material with $\rho = 2000$ kg/m^3, $V_s = 1000$ m/s and $\nu = 0.3$ (corresponding to $G = 2$ GPa). No Rayleigh damping has been introduced.

As for the input motion, two different Ormsby wavelets have been employed, corresponding with the following input parameters in Equation (5):

[3]Henceforth, Δx will always denote the vertical node spacing, coinciding with the element thickness in the case of 8-node bricks.

– input 1: f_1=0.1 Hz, f_2=1 Hz, f_3=18 Hz, f_4=20 Hz (plotted in Figure 2);

– input 2: f_1=0.1 Hz, f_2=1 Hz, f_3=45 Hz, f_4=50 Hz;

– the amplitude parameter A has been always set to produce at the bottom layer a maximum displacement of 1 mm.

As previously mentioned (section 2.3), both inputs 1 and 2 have been used to explore the interplay between discretization effects and the width of the frequency range.

3.3 Discussion of numerical results

The influence of grid spacing and time-step size are discussed separately for the sake of clarity. Since the Real ESSI program is based on a displacement FE formulation, displacement components are the most reliable output; however, some consideration is also paid to accelerations, post-calculated through second-order central differentiation.

Table 1 provides a list of the comparative simulations performed for fully linear problems. Each case is denoted by: (i) maximum frequency f_{max} in the input wavelet (f_4 in (5)); (ii) standard grid spacing Δx_{std} and (iii) time-step size Δt_{std} from discretization rules (10)–(11); (iv) Δx and (v) Δt actually used; (vi) type of brick elements adopted.

case #	f_{max} [Hz]	Δx_{std} [m]	Δt_{std} [s]	Δx [m]	Δt [s]	brick type
EL1	20	5	0.005	2, 5, 10	0.005	8-node
EL2	20	5	0.005	2, 5, 10	0.002	8-node
EL3	50	2	0.002	0.8, 2, 4	0.002	8-node
EL4	50	2	0.002	0.8, 2, 4	0.001	8-node
EL5	20	5	0.005	2, 5, 10	0.002	27-node
EL6	20	5	0.005	5	0.002, 0.005, 0.01	8-node
EL7	20	5	0.005	2	0.001, 0.002, 0.005	8-node
EL8	50	2	0.002	2	0.001, 0.002, 0.005	8-node
EL9	50	2	0.002	0.8	0.0005, 0.001, 0.002	8-node
EL10	20	5	0.005	5	0.002, 0.005, 0.01	27-node

Table 1: List of elastic simulations

The results being presented aim to assess the quality of standard discretization rules, as well as the improvements attainable through refined discretization. For this purpose, the numerical results are discussed in both time and frequency domains – the Fourier spectra of considered time histories are plotted in terms of (i) amplitude and (ii) phase difference with respect to the analytical solution (known at the free surface). **Additional quantitative insight is also gained**

through the EM and PM misfit criteria introduced in section 2.4. Unless differently stated, numerical outputs at the top of the soil layer are considered.

3.3.1 Influence of grid spacing

Grid spacing effects at the top of the FE model are illustrated in Figures 3–6 for the cases EL1–EL5 (Table 1) in terms of: (a–b) displacement time histories; (c) Fourier amplitudes and (d) phase differences at the surface; (e) EM and PM misfits (for each numerical solution, misfits are calculated with respect to the exact analytical solution). Starting from Figure 4, displacement time histories are not compared with the input motion (as done in Figure 3(a)) for the sake of brevity, whereas only a reduced time window around the output motion is displayed for a clearer visualisation (e.g. as in Figure 3(b))

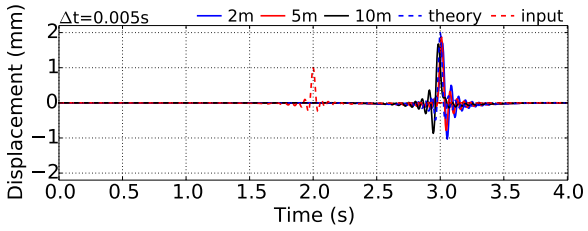

(a) Displacement time history (0.0-4.0 s)

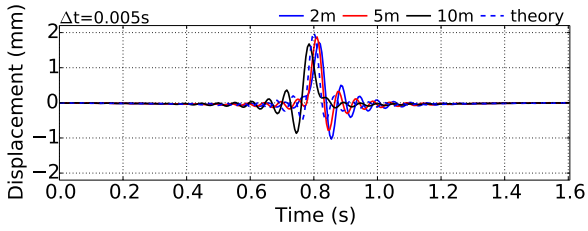

(b) Displacement time history (2.2–3.8 s)

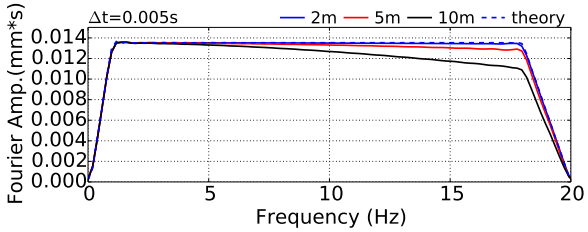

(c) Amplitude of displacement Fourier spectrum

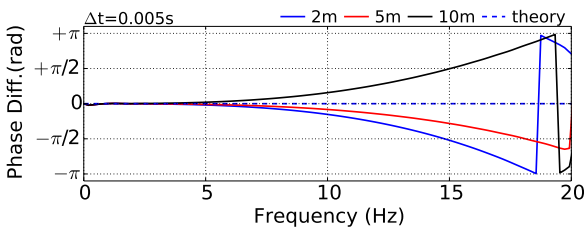

(d) Phase difference of displacement Fourier spectrum

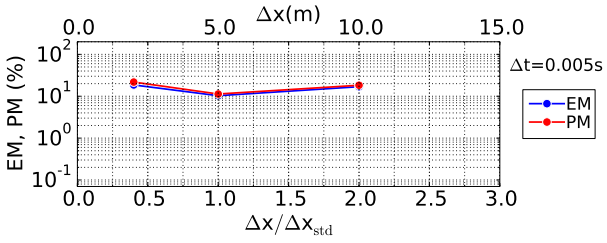

(e) EM/PM misfits (ref. solution: analytical)

Figure 3: Influence of grid spacing, displacement plot, case EL1 ($f_{max} = 20$ Hz, $\Delta x_{std} = 5$ m, $\Delta t_{std} = 0.005$ s, $\Delta x = 2$, 5, 10 m, $\Delta t = 0.005$ s, 8-node brick)

Figures 3–6 suggest the following observations (some of which expected):

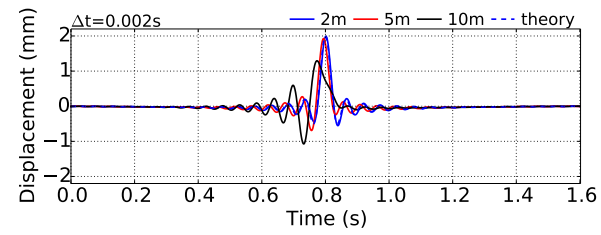

(a) Displacement time history (2.2-3.8 s)

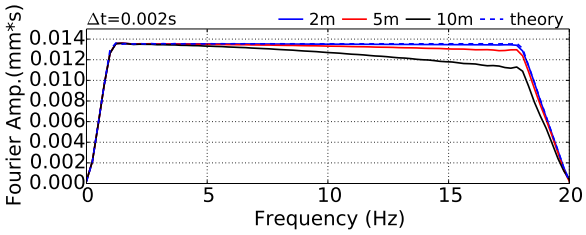

(b) Amplitude of displacement Fourier spectrum

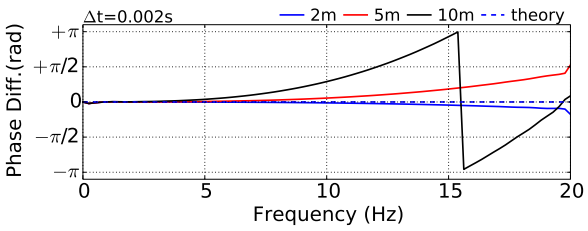

(c) Phase difference of displacement Fourier spectrum

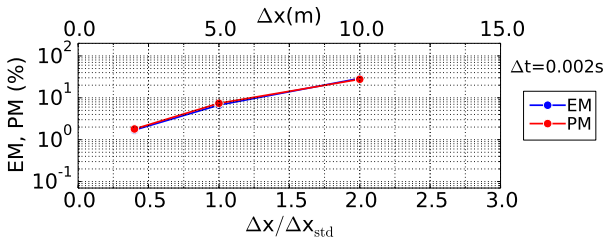

(d) EM/PM misfits (ref. solution: analytical)

Figure 4: Influence of grid spacing, displacement plot, case EL2 ($f_{max} = 20$ Hz, $\Delta x_{std} = 5$ m, $\Delta t_{std} = 0.005$ s, $\Delta x = 2$, 5, 10 m, $\Delta t = 0.002$ s, 8-node brick)

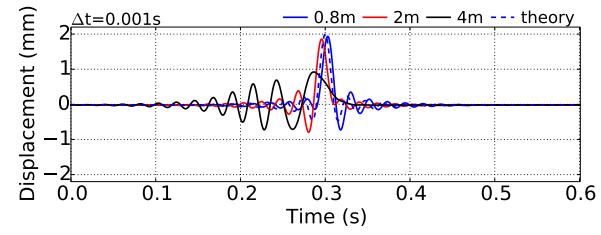

(a) Displacement time history (2.2-2.8 s)

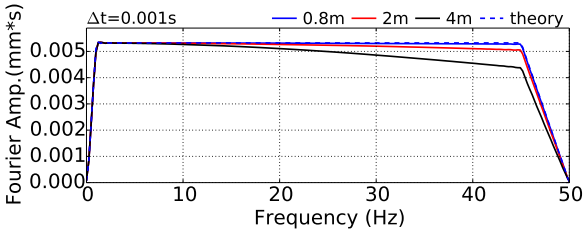

(b) Amplitude of displacement Fourier spectrum

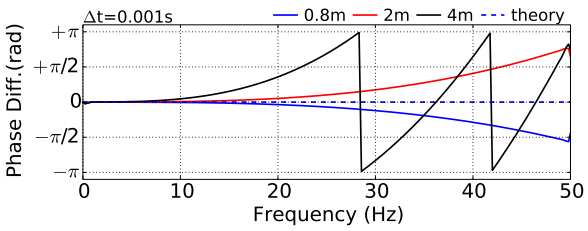

(c) Phase difference of displacement Fourier spectrum

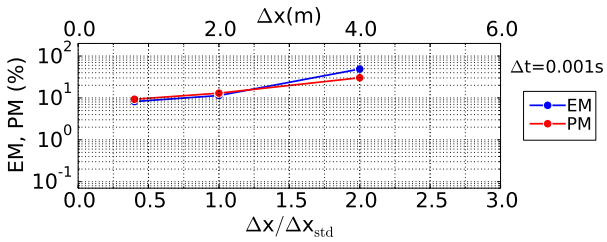

(d) EM/PM misfits (ref. solution: analytical)

Figure 5: Influence of grid spacing, displacement plot, case EL4 ($f_{max} = 50$ Hz, $\Delta x_{std} = 2$ m, $\Delta t_{std} = 0.002$ s, $\Delta x = 0.8$, 2, 4 m, $\Delta t = 0.001$ s, 8-node brick)

– **even though Δx_{std} is set on the basis of the maximum frequency f_{max}, its suitability as grid spacing is not uniform over the input spectrum. Indeed, increasing inaccuracies in the frequency domain are clearly visible as f_{max} is approached (check for instance the Fourier amplitudes compared in Figures 3(c) and 4–**

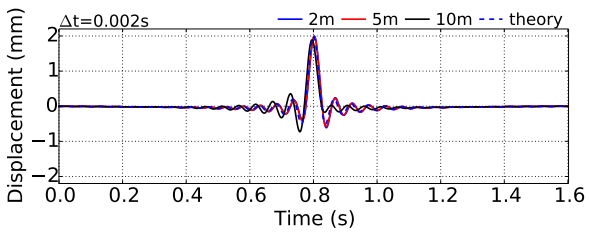

(a) Displacement time history (2.2–3.8 s)

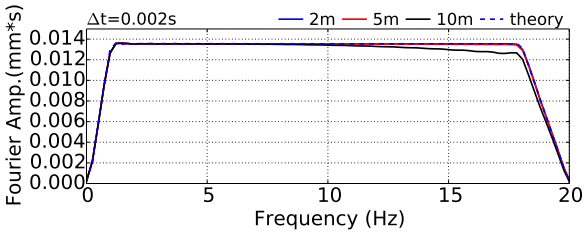

(b) Amplitude of displacement Fourier spectrum

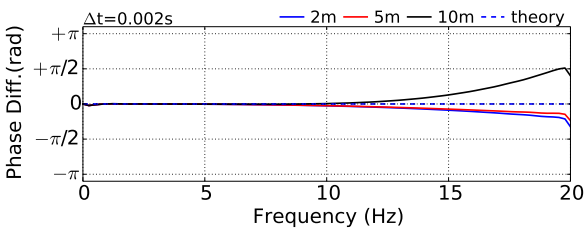

(c) Phase difference of displacement Fourier spectrum

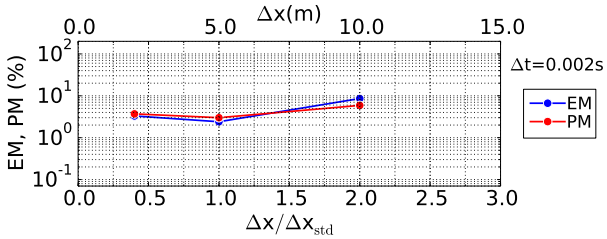

(d) EM/PM misfits (ref. solution: analytical)

Figure 6: Influence of grid spacing, displacement plot, case EL5 ($f_{max} = 20$ Hz, $\Delta x_{std} = 5$ m, $\Delta t_{std} = 0.005$ s, $\Delta x = 2$, 5, 10 m, $\Delta t = 0.002$ s, 27-node brick)

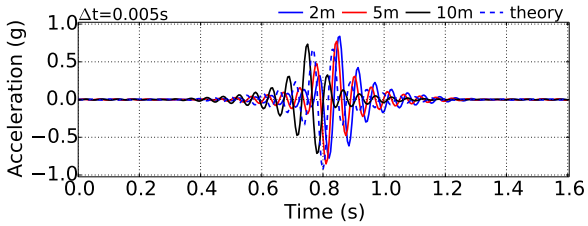

(a) Acceleration time history (2.2– 3.8 s)

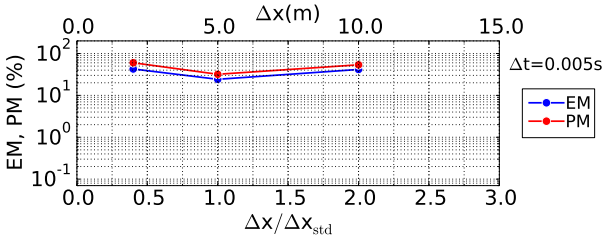

(b) EM/PM misfits (ref. solution: analytical)

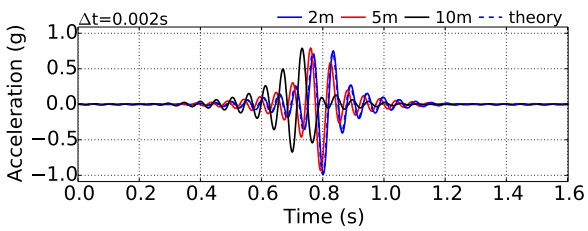

(c) Acceleration time history (2.2– 3.8 s)

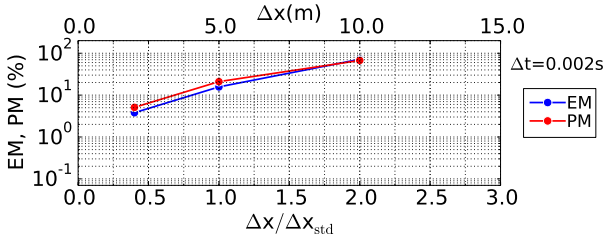

(d) EM/PM misfits (ref. solution: analytical)

Figure 7: Influence of grid spacing, acceleration plot, cases (a–b) EL1 ($f_{max} = 20$ Hz, $\Delta x_{std} = 5$ m, $\Delta t_{std} = 0.005$ s, $\Delta x = 2$, 5, 10 m, $\Delta t = 0.005$ s, 8-node brick) and (c–d) EL2 ($f_{max} = 20$ Hz, $\Delta x_{std} = 5$ m, $\Delta t_{std} = 0.005$ s, $\Delta x = 2$, 5, 10 m, $\Delta t = 0.002$ s, 8-node brick)

6(b)). Grid spacing affects output Fourier spectra both in amplitude and phase;

– in all cases, envelope and phase misfits, EM and PM, are quantitatively very

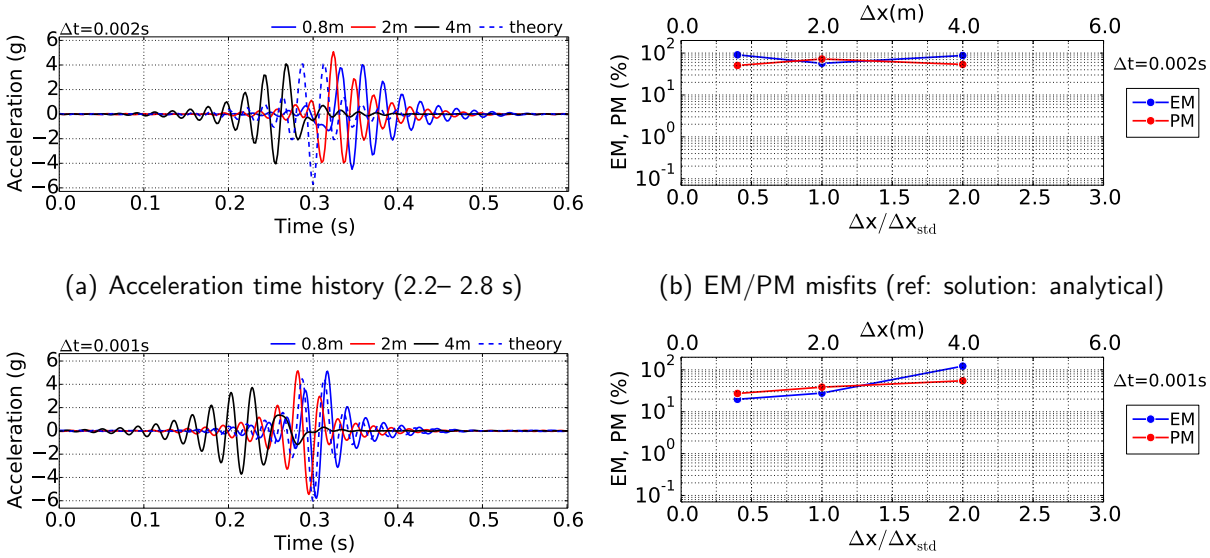

(a) Acceleration time history (2.2– 2.8 s)

(b) EM/PM misfits (ref: solution: analytical)

(c) Acceleration time history (2.2– 2.8 s)

(d) EM/PM misfits (ref: solution: analytical)

Figure 8: Influence of grid spacing, acceleration plot, cases (a–b) EL3 ($f_{max} = 50$ Hz, $\Delta x_{std} = 2$ m, $\Delta t_{std} = 0.002$ s, $\Delta x = 0.8$, 2, 4 m, $\Delta t = 0.002$ s, 8-node brick) and (c–d) EL4 ($f_{max} = 50$ Hz, $\Delta x_{std} = 2$ m, $\Delta t_{std} = 0.002$ s, $\Delta x = 0.8$, 2, 4 m, $\Delta t = 0.001$ s, 8-node brick)

similar (Figures 3(e) and 4–6(d));

- **reducing Δx below Δx_{std} is beneficial only if Δt is also lower than Δt_{std}. This is apparent in Figure 3(e), where an increase in EM and PM is observed as Δx gets lower than Δx_{std}. Conversely, monotonic EM/PM trends are shown in Figures 4–5(d);**

- **at given grid spacing Δx, reducing the time-step improves the numerical solution mostly in terms of Fourier phase, not amplitude (compares Figures 3(c–d) and 4(b–c)). It may be generally stated that, when Δx is not appropriate, reducing the time-step size does not produce substantial improvements;**

- **based on these initial examples, a grid spacing Δx in the order of $V_s/20f_{max} = \Delta x_{std}/2$ ensures high accuracy (EM and PM <10%) in combination with $\Delta t = \Delta x/2V_s = \Delta t_{std}/2$. These enhanced discretization rules hold for low-order FEs (8-node brick elements) but are not affected by the frequency bandwidth of the input signal. In the latter respect, Figures 4–5(d) show quantitatively similar EM-PM trends for f_{max} equal to 20 Hz and 50 Hz. Also, minimum misfits are attained in the EL2 case, where a smaller $\Delta t/\Delta t_{std}$ ratio has been purposely set.**

The above conclusions apply to 8-node brick elements, while Figure 6 shows that

"ten nodes per wavelength" are still suitable when higher–order elements (here 27-node bricks[4]) are employed. However, this lighter requirement for grid spacing seems to perform well in combination with $\Delta t \leq \Delta x/2V_s$, and results in EM and PM lower than 10% even for $\Delta x/\Delta x_{std} = 2$ (5 nodes per wavelength).

It is also important to evaluate grid spacing effects on acceleration components, as they will affect the inertial forces transmitted to manmade structures on the ground surface. Since acceleration time histories are dominated by high frequencies, the poorer performance of standard discretization rules at high frequencies becomes more evident. In Figures 7 and 8, grid spacing plays qualitatively as in Figures 3–5, though the EM/PM trends – similar in shape – are shifted upwards. This means that, in the presence of low–order elements, more severe discretization requirements should be fulfilled if very accurate accelerations need to be computed.

3.3.2 Influence of time-step size

For given grid spacings, the influence of Δt has been studied by varying the time-step size with respect to the limit emerging from Equation (11), i.e. $\Delta t_{std} = \Delta x/V_s$. Time discretization effects are illustrated in Figures 9-14 and suggest the following comments:

- as observed in the previous subsection, Δt mainly affects the Fourier phase, **with comparable EM and PM values in all cases**. Phase differences with respect to the exact solution decrease as Δt is reduced – see for instance in Figures 9-12(c);

- **in combination with $\Delta x = V_s/20f_{max} = \Delta x_{std}/2$, $\Delta t = \Delta t_{std}$ may still result in some high-frequency phase-difference with the respect to the analytical solution, (Figures 9-12(c)). As found by investigating grid spacing effects, $\Delta t = \Delta x/2V_s = \Delta t_{std}/2$ yields sufficient accuracy (EM-PM lower than 10%) to most practical purposes (see Figures 9-12(d))**;

- **when 27-node bricks are used, the use of $\Delta x = \Delta x_{std}$ and $\Delta t \leq \Delta t_{std}/2$ is still an appropriate option, giving rise to EM and PM lower than 5% (Figures 12). Even in this case, discretization errors are still governed by phase differences, while excellent performance in terms of Fourier amplitude is observed**;

- **Figures 13 and 14 show that the above inferences apply qualitative to acceleration time histories as well. However, EM and PM value are quite high (significantly larger than 10%) while $\Delta t \geq \Delta t_{std}$, regardless of the grid spacing ratio. Accuracy is quickly gained when Δt is reduced and $\Delta x < \Delta x_{std}/2$.**

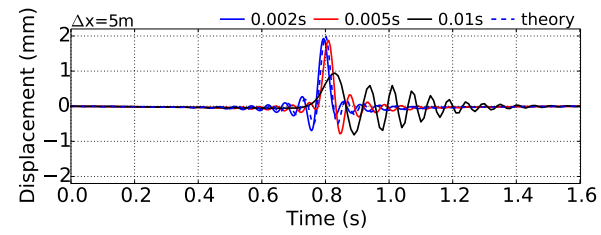

(a) Displacement time history (2.2–3.8 s)

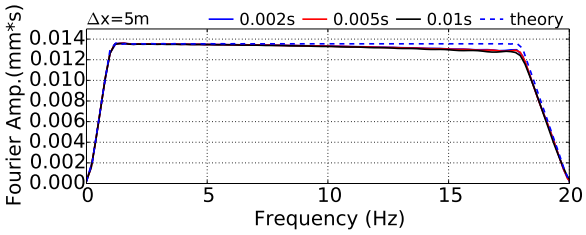

(b) Amplitude of displacement Fourier spectrum

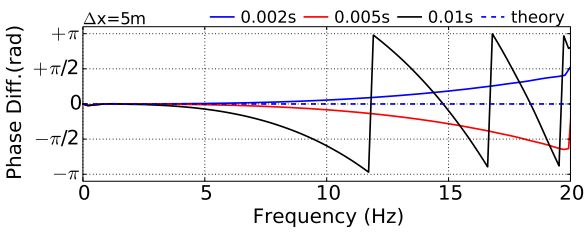

(c) Phase difference of displacement Fourier spectrum

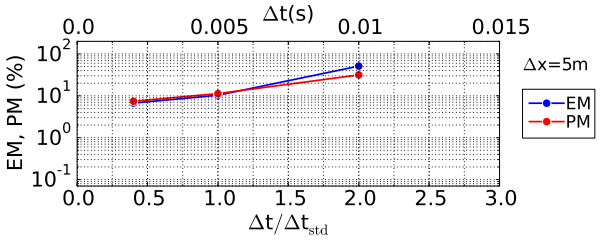

(d) EM/PM misfits (ref: solution: analytical)

Figure 9: Influence of time-step size, displacement plot, case EL6 ($f_{max} = 20$ Hz, $\Delta x_{std} = 5$ m, $\Delta t_{std} = 0.005$ s, $\Delta x = 5$ m, $\Delta t =$ 0.002, 0.005, 0.010 s, 8-node brick)

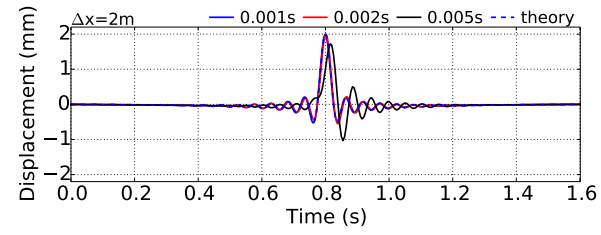

(a) Displacement time history (2.2–3.8 s)

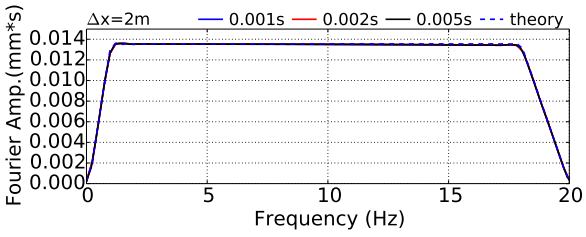

(b) Amplitude of displacement Fourier spectrum

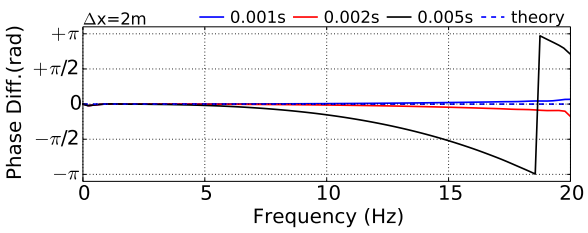

(c) Phase difference of displacement Fourier spectrum

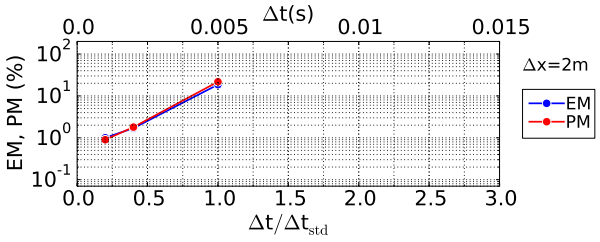

(d) EM/PM misfits (ref: solution: analytical)

Figure 10: Influence of grid spacing, displacement plot, case EL7 ($f_{max} = 20$ Hz, $\Delta x_{std} = 5$ m, $\Delta t_{std} = 0.005$ s, $\Delta x = 2$ m, $\Delta t =$ 0.001, 0.002, 0.005 s, 8-node brick)

While the above conclusions have been all drawn on the basis of the first incoming wave, many reflected waves may in reality hit the ground surface because of soil layering. In the

[4] **For a given number of nodes per wavelength, the size Δx of 27-node elements along the propagation direction is double than for 8-node bricks.**

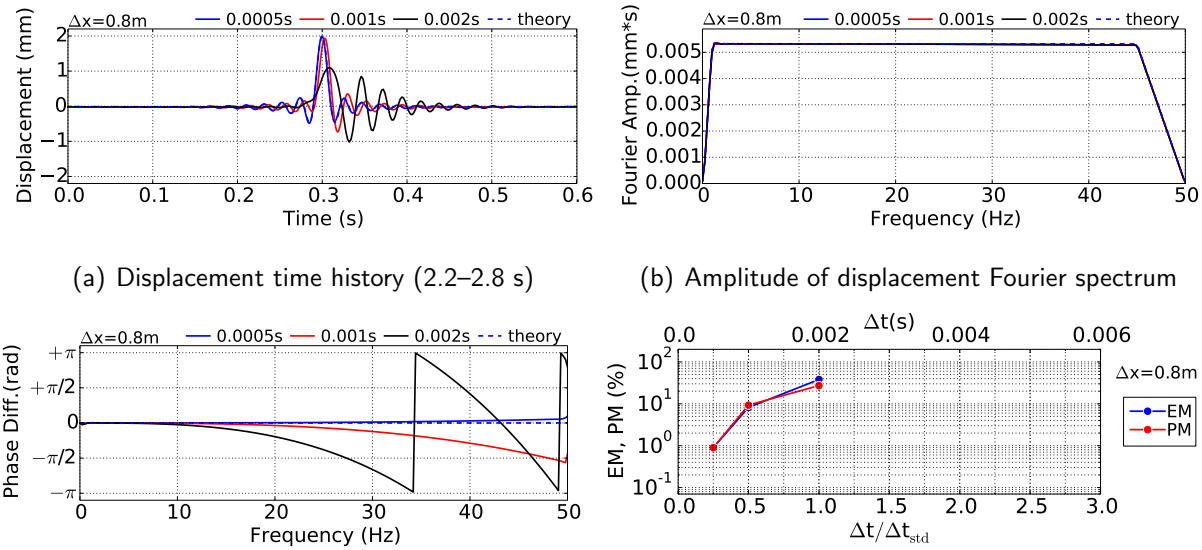

(a) Displacement time history (2.2–2.8 s)

(b) Amplitude of displacement Fourier spectrum

(c) Phase difference of displacement Fourier spectrum

(d) EM/PM misfits (ref: solution: analytical)

Figure 11: Influence of time-step size, displacement plot, case EL9 ($f_{max} = 50$ Hz, $\Delta x_{std} = 2$ m, $\Delta t_{std} = 0.002$ s, $\Delta x = 0.8$ m, $\Delta t =$ 0.0005, 0.001, 0.002 s, 8-node brick)

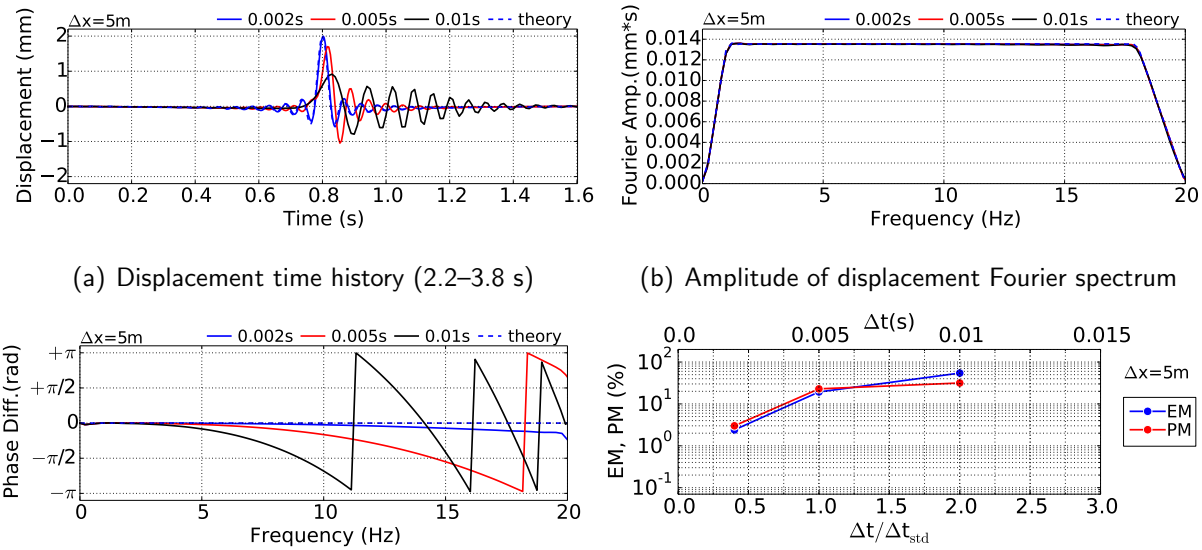

(a) Displacement time history (2.2–3.8 s)

(b) Amplitude of displacement Fourier spectrum

(c) Phase difference of displacement Fourier spectrum

(d) EM/PM misfits (ref: solution: analytical)

Figure 12: Influence of time-step size, displacement plot, case EL10 ($f_{max} = 20$ Hz, $\Delta x_{std} = 5$ m, $\Delta t_{std} = 0.005$ s, $\Delta x = 5$ m, $\Delta t =$ 0.002, 0.005, 0.010 s, 27-node brick)

present elastic case (no energy dissipation), perfect reflections occur at the lower rigid bedrock and never-ending wave motion is established. It is thus interesting to check how discretization errors propagate in time at the free surface, as is shown in Figure 15. Subsequent wave arrivals are compared in the time (Figure 15(a)-(b)) and frequency (Figure 15(c)-(d)) domains, where a

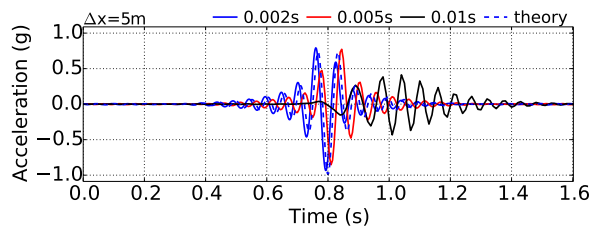

(a) Acceleration time history (2.2–3.8 s)

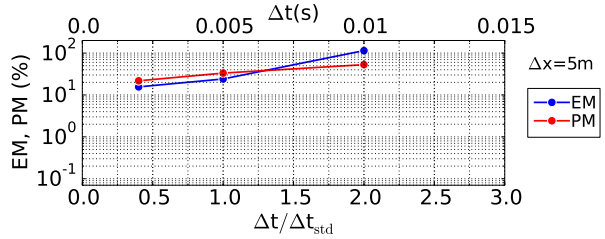

(b) EM/PM misfits (ref: solution: analytical)

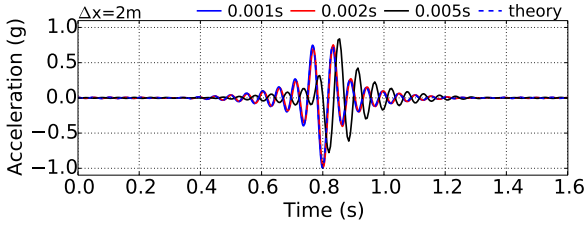

(c) Acceleration time history (2.2–3.8 s)

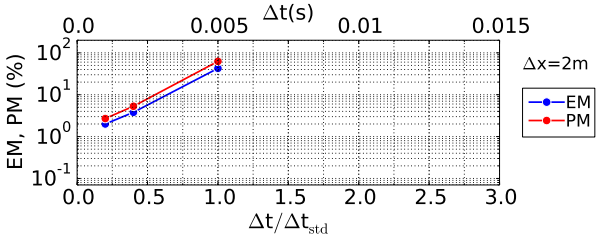

(d) EM/PM misfits (ref: solution: analytical)

Figure 13: Influence of time-step size, acceleration plot, cases EL6 ($f_{max} = 20$ Hz, $\Delta x_{std} = 5$ m, $\Delta t_{std} = 0.005$ s, $\Delta x = 5$ m, $\Delta t =$ 0.002, 0.005, 0.010 s, 8-node brick) and EL7 ($f_{max} = 20$ Hz, $\Delta x_{std} = 5$ m, $\Delta t_{std} = 0.005$ s, $\Delta x = 2$ m, $\Delta t =$ 0.001, 0.002, 0.005 s, 8-node brick)

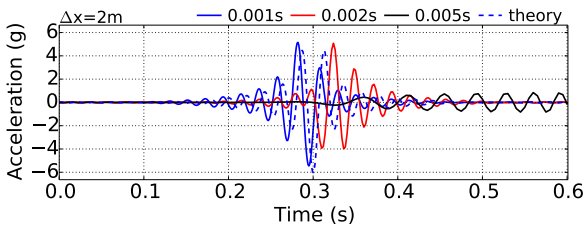

(a) Acceleration time history (2.2–2.8 s)

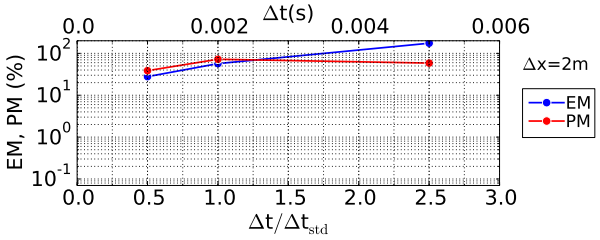

(b) EM/PM misfits (ref: solution: analytical)

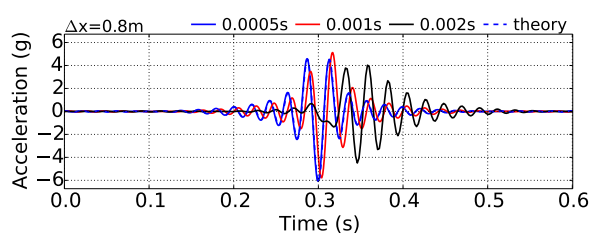

(c) Acceleration time history (2.2–2.8 s)

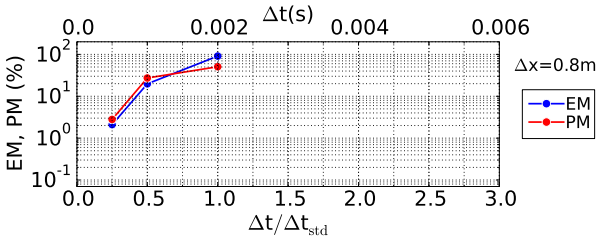

(d) EM/PM misfits (ref: solution: analytical)

Figure 14: Influence of time-step size, acceleration plot, cases EL8 ($f_{max} = 50$ Hz, $\Delta x_{std} = 2$ m, $\Delta t_{std} = 0.002$ s, $\Delta x = 2$ m, $\Delta t =$ 0.001, 0.002, 0.005 s, 8-node brick) and EL9 ($f_{max} = 50$ Hz, $\Delta x_{std} = 2$ m, $\Delta t_{std} = 0.002$ s, $\Delta x = 0.8$ m, $\Delta t =$ 0.0005, 0.001, 0.002 s, 8-node brick)

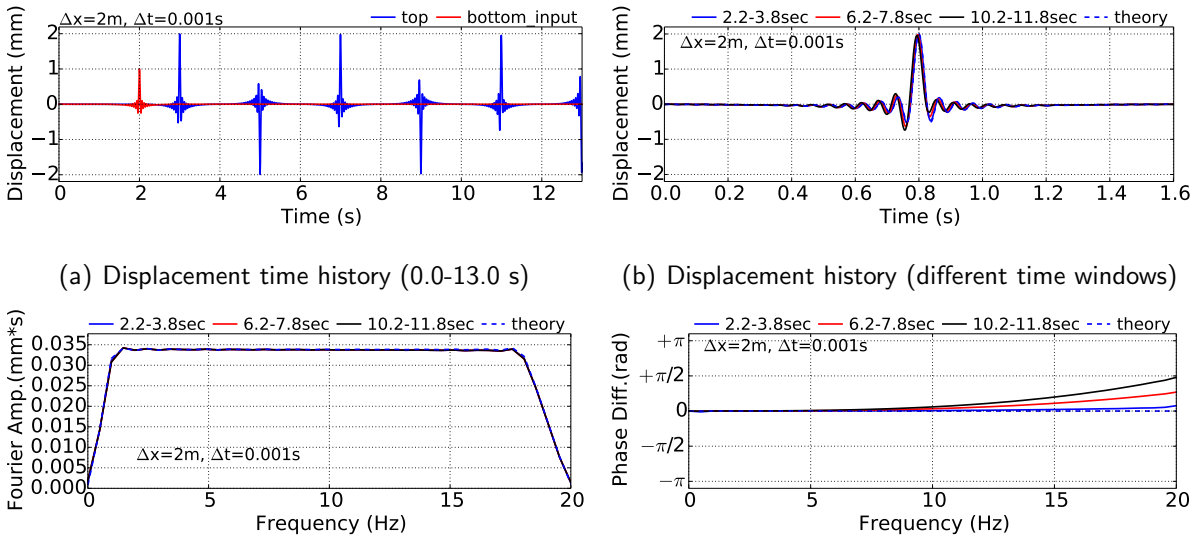

(a) Displacement time history (0.0-13.0 s)

(b) Displacement history (different time windows)

(c) Amplitude of displacement Fourier spectrum

(d) Phase difference of displacement Fourier spectrum

Figure 15: Time evolution of wave dispersion, displacement plot, case EL7 ($f_{max} = 20$ Hz, $\Delta x_{std} = 5$ m, $\Delta t_{std} = 0.005$ s, $\Delta x = 2$ m, $\Delta t = 0.001$ s, 8-node brick)

gradual "accumulation" of wave dispersion can be observed. Even though satisfactory accuracy is achieved on the first arrival, an increase in high-frequency phase difference is detected in Figure 15(d), with negligible variation in Fourier amplitude (Figure 15(c)). The effect of cumulative wave dispersion is apparent in Figure 15(a), and implies that selecting suitable Δx and Δt becomes increasingly delicate for large FE models and long durations.

4 Non-linear elastic-plastic wave simulations

This section concerns discretization effects in presence of material non-linearity. As most commonly done in Geomechanics (Zienkiewicz et al., 1999), the non-linear cyclic response of geomaterials can be described in the framework of elasto-plasticity, and here the VMKH and PM models described in Section 2.2 have been adopted. Prior to presenting numerical results, some preliminary remarks should be made:

- the non-linear problem under consideration cannot be solved analytically. Therefore, the quality of discretization settings may only be assessed by evaluating the converging behavior of numerical solutions upon Δx–Δt refinement;

- with no analytical solution at hand, one needs engineering judgement to establish when the (unknown) exact solution is reasonably approached. In this respect, light is shed hereafter on several expected pitfalls, all relevant to the global verification process (Oberkampf et al.,

2004; Babuska and Oden, 2004; Roy and Oberkampf, 2011);

– the accuracy of non-linear computations is highly affected by the input amplitude. This governs the amount of non-linearity mobilized by wave motion and, as a consequence, the accuracy of numerical solutions at varying discretization.

In non-linear (elastic-plastic) problems, discretization is not only responsible for the numerical representation of waves (dissipation, dispersion, stability), but also governs the accuracy of constitutive integration (Simo and Hughes, 1998; Borja, 2013). For instance, changes in time-step size will affect the strain size driving the constitutive integration algorithm and, in turn, the final simulation results. This dependence of the constitutive response (material model and constitutive integration algorithm) on the dynamic step size precludes direct development of automatic criteria for discretization. However, as tangent elastic-plastic response can be established for any stress-strain combination, (lowest) elastic-plastic (shear) stiffness may be used to develop suitable discretization via Equation 4. Apparently, this approach assumes that the stress-strain response is already known, as is not the case when discretization is being set. This means that an iterative approach is in principle needed, whereby one will first design discretization based on an estimate of the strain level, run the dynamic simulation, and record the actual stress-strain response. After few iterations, a stable discretization will be usually achieved.

In this study, VMKH and PM constitutive equations have been integrated via the standard forward Euler, explicit algorithm (Desai and Siriwardane, 1984; Chen and Han, 1988). Although implicit algorithms may possess better accuracy/stability properties, explicit integration is often preferred for advanced constitutive formulations and cyclic loading (Jeremić et al., 2008). There is also wide consensus on the poor performance in elastic-plastic computations of time-step sizes derived through elastic parameters and Equation (11), especially in combination with explicit stress-point algorithms. For this reason, the following time marching rule may be regarded as an upper bound for non-linear problems (instead of (11)):

$$\Delta t \leq \frac{\Delta x}{10 V_s} \tag{12}$$

In the following, rules (10) and (12) will be assumed as starting discretization criteria and critically assessed. For shorter discussion, only input 1 (f_{max} = 20 Hz) and 8-node brick elements are employed for non-linear simulations.

4.1 VMKH model

4.1.1 Model parameters and parametric analysis

A heterogeneous 1 km thick soil deposit has been considered, formed by a 200 m thick VMKH sub-layer resting on an elastic stratum (remaining 800 m). At the surface, a thin layer (5 m)

of elastic material has been added to prevent numerical problems with very strong motions and the so-called whip effect. The following constitutive parameters (see Section 2.2.2) have been set (same elastic parameters for both the VMKH and the elastic sub-layers), with no algorithmic nor Rayleigh damping introduced in numerical computations.:

- mass density and elastic properties: $\rho = 2000$ kg/m^3, $E = 5.2$ GPa and $\nu = 0.3$, whence the elastic shear wave velocity $V_s = 1000$ m/s results (same elastic parameters employed for both the elastic and the VMKH sub-layers);
- yielding parameter (radius of the von Mises cylinder): $k = 10.4$ kPa;
- different h values (hardening parameter) have been set: $h = 0.5E$, $0.05E$, $0.01E$.

In the analysis of VMKH cases, the influence of the hardening parameter (h) and the input amplitude (A) is also considered, as they affect the material elastic-plastic stiffness and the amount of plasticity mobilized. The VMKH simulation programme is reported in Table 2, where Δt_{std} has been determined through Equation (12) (i.e. $\Delta t_{std} = \Delta x / 10 V_s$).

case #	Δx_{std} [m]	Δt_{std} [s]	Δx [m]	Δt [s]	h	A [mm]
VMKH1	5	0.0005	1, 5	0.0001	$0.5E$	0.1
VMKH2	5	0.0005	1, 5	0.0001	$0.05E$	0.1
VMKH3	5	0.0005	5	0.0002, 0.0005, 0.001	$0.5E$	0.1
VMKH4	5	0.0005	5	0.0002, 0.0005, 0.001	$0.05E$	0.1
VMKH5	5	0.0005	5	0.0002, 0.0005, 0.001	$0.01E$	0.1
VMKH6	5	0.0005	1, 5	0.0001	$0.5E$	1
VMKH7	5	0.0005	1, 5	0.0001	$0.05E$	1
VMKH8	5	0.0005	5	0.0002, 0.0005, 0.001	$0.5E$	1
VMKH9	5	0.0005	5	0.0002, 0.0005, 0.001	$0.05E$	1
VMKH10	5	0.0005	5	0.0002, 0.0005, 0.001	$0.01E$	1

Table 2: List of VMKH simulations

4.1.2 Influence of grid spacing and time-step size

The results in Figures 16 and 17 exemplify the role played by space discretization in elastic-plastic simulations. These results have been obtained by employing a time-step smaller than Δt_{std} (cases VMKH1–2 in Table 2), a low input amplitude ($A = 0.1$ mm corresponds with a peak ground acceleration approximately equal to $0.05g$), and two different values of the hardening parameter ($h = 0.5E$ and $h = 0.05E$). The following observations arise from the two figures:

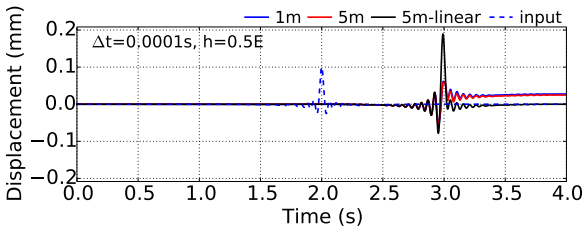

(a) Displacement time history (0.0–4.0 s)

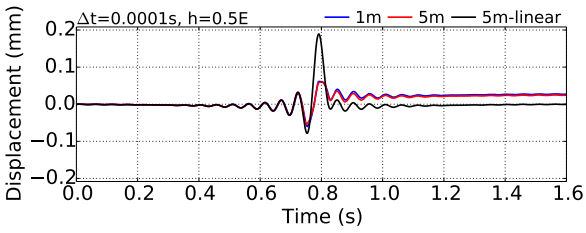

(b) Displacement time history (2.2–3.8 s)

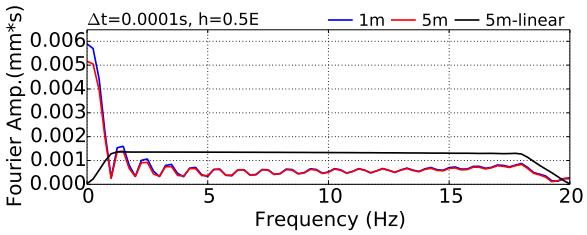

(c) Amplitude of displacement Fourier spectrum

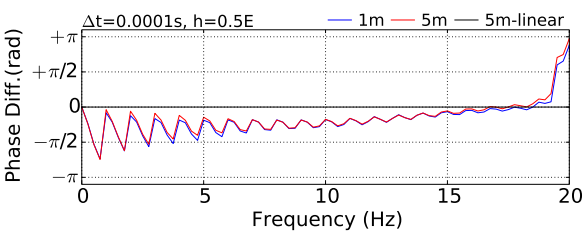

(d) Phase difference of displacement Fourier spectrum

Figure 16: Influence of grid spacing, displacement plot, case VMKH1 ($\Delta x_{std} = 5$ m, $\Delta t_{std} = 0.0005$ s, $\Delta x = 1$, 5 m, $\Delta t = 0.0001$ s, $h = 0.5E$, $A = 0.1$ mm)

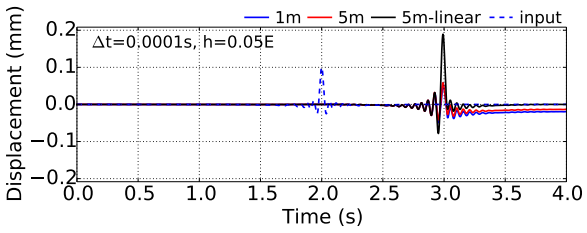

(a) Displacement time history (0.0–4.0 s)

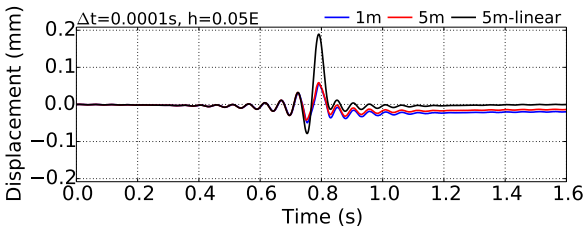

(b) Displacement time history (2.2–3.8 s)

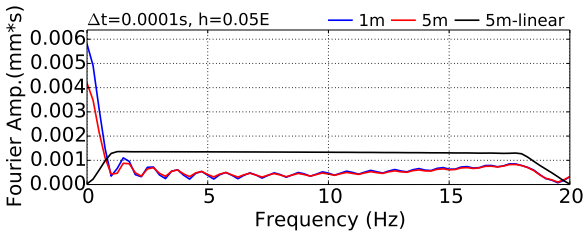

(c) Amplitude of displacement Fourier spectrum

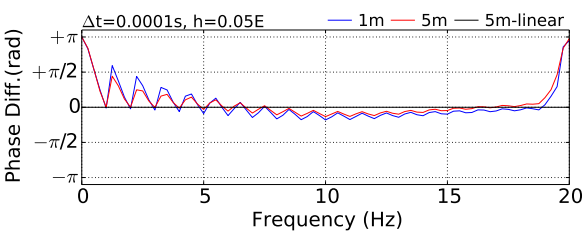

(d) Phase difference of displacement Fourier spectrum

Figure 17: Influence of grid spacing, displacement plot, case VMKH2 ($\Delta x_{std} = 5$ m, $\Delta t_{std} = 0.0005$ s, $\Delta x = 1$ m, 5 m, $\Delta t = 0.0001$ s, $h = 0.05E$, $A = 0.1$ mm)

– **propagation through a dissipative elastic-plastic material alters significantly the appearance of the input signal. All plots display significant wave attenuation/distortion, while final unrecoverable displacements are produced by soil plastifications (Figures 16–17(a)). Steady irreversible deformations are associated**

with prominent static components (at nil frequency) in the Fourier amplitude spectrum (Figures 16–17(c)), not present in the input Ormsby wavelet (Figure 2(b));

- **the numerical representation of wavelengths is dominated by soil plasticity, producing more deviation from the input waveform than variations in grid spacing. For this reason, only two Δx values have been used in this subsection for illustrative purposes, whereas EM/PM plots have been deemed not necessary;**

- **the influence of Δx seems slightly magnified when lower h values, and thus lower elastic-plastic stiffness, are set (see Figure 17). It is indeed not surprising that wave propagation in softer media may be more strictly affected by space discretization, as in linear problems. However, it should be noted that Δx mainly influences the final irreversible displacement (Figure 17(b)-(c)), which leads to presume substantial interplay of grid effects and constitutive time integration;**

- **since the effects of Δx reduction are quite small in both time and frequency domains (for a given Δt), there is no strong motivation to suggest $\Delta x = V_s/20 f_{max}$. $\Delta x = V_s/10 f_{max} = \Delta x_{std}$ should be actually appropriate in common practical situations, as long as no soil failure mechanisms are triggered – as e.g. in seismic slope stability problems (di Prisco et al., 2012). The occurrence of soil failure may introduce additional discretization requirements for an accurate kinematic representation of collapse.**

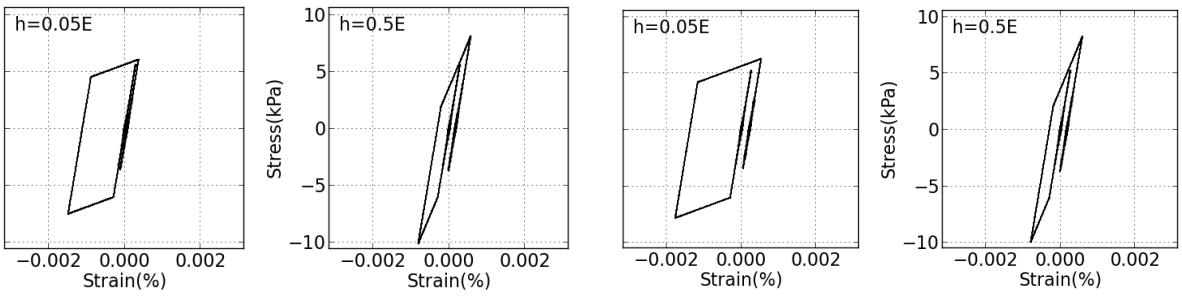

(a) Δx=5 m (b) Δx=1 m

Figure 18: Influence of grid spacing, shear stress-strain response at the bottom of the VMKH sub-layer, cases VMKH1 ($h = 0.5E$) and VMKH2 ($h = 0.05E$), ($\Delta x_{std} = 5$ m, $\Delta t_{std} = 0.0005$ s, $\Delta t = 0.0001$ s, $A = 0.1$ mm)

In addition, Figure 18 illustrates the shear stress-strain VMKH response at the deepest integration (Gauss) point of the VMKH sub-layer. The material response is bilinear (elastic and

elastic-plastic), with the elastic stiffness recovered upon stress reversal until new yielding occurs (Lemaitre and Chaboche, 1990). As mentioned above, the observable (small) difference in stress-strain response at different Δx may not be straightforwardly attributed to grid spacing deficiencies, but rather to the coupled influence of discretization in space and time on the global dynamics of the system.

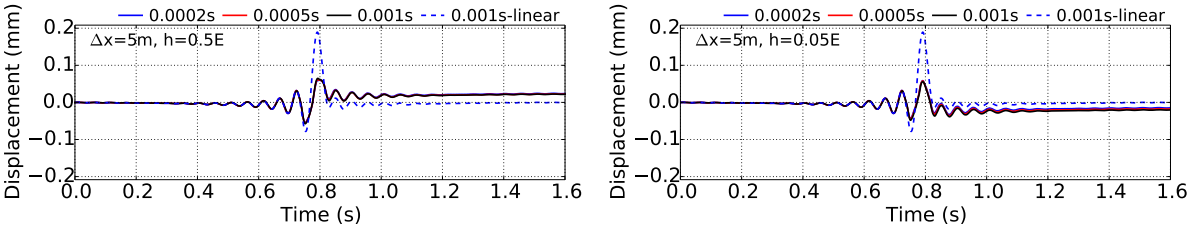

(a) Displacement time history, $h = 0.5E$ (2.2–3.8 s) (b) Displacement time history, $h = 0.05E$ (2.2–3.8 s)

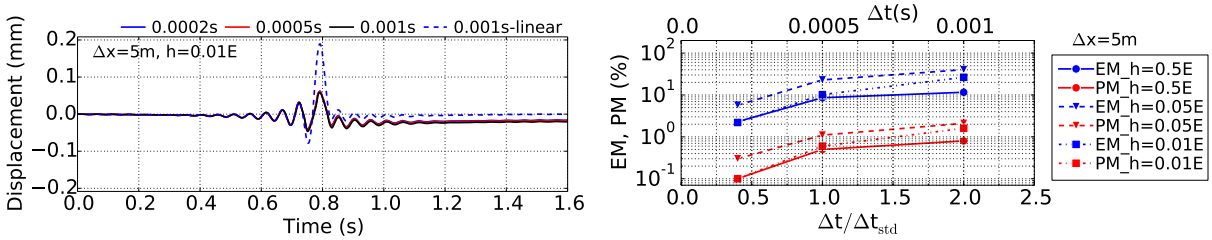

(c) Displacement time history, $h = 0.01E$ (2.2–3.8 s) (d) EM/PM misfits (ref. solution: $\Delta t = 0.0001$ s)

Figure 19: Influence of time-step size, displacement plot, cases VMKH3 ($h = 0.5E$), VMKH4 ($h = 0.05E$) and VMKH5 ($h = 0.01E$) ($\Delta x_{std} = 5$ m, $\Delta t_{std} = 0.0005$ s, $\Delta x = 5$ m, $\Delta t =$ 0.0002, 0.0005, 0.001 s, $A = 0.1$ mm)

The influence of the time-step size is illustrated for cases VMKH3–5 (Table 2) in Figures 19–20, encompassing three h values ($0.5E$, $0.05E$ and $0.01E$) and also including EM/PM plots (Figure 19(d)). In the lack of analytical solutions, misfits have been determined on the basis of a "sufficiently accurate" reference solution, here obtained numerically by setting $\Delta t = \Delta t_{std}/5 =$ 0.0001 s. For a relatively small input amplitude ($A =$ 0.1 mm), convergence seems overall quite fast, and even $\Delta t = \Delta t_{std}$ results in both EM and PM values lower or close to 10% (in combination with $\Delta x = \Delta x_{std}$). This inference is further corroborated by the shear stress-strain response at the bottom of the VMKH sub-layer (Figure 20), exhibiting little sensitiveness to the time-step size. Some additional comments stem from the EM/PM plots in Figure 19(d):

- **at variance with the previous elastic cases, envelope (EM) and phase (PM) misfits are quantitatively quite different (EM>PM);**
- **EM/PM trends do not depend monotonically on the hardening parameter h. For**

$\Delta t =$ **0.0002 s, the EM/PM values at** $h = 0.05E$ **are indeed larger than the those obtained for** $h = 0.5E$ **and** $h = 0.01E$.

Both findings are likely to relate to the influence of time discretization on the residual displacement, which is larger than on other response features. In fact, variations in the accumulated displacement mainly affect the envelope of the output signal, not its phase attributes. The counterintuitive non-monotonic relationship between h **and displacement EM/PM values has not been detected in the corresponding acceleration EM/PM plots (not reported here), due to the obvious lack of residual accelerations.**

4.1.3 Influence of input motion amplitude

In non-linear problems, it is hard to draw general conclusions on the interaction between space/time discretization and input amplitude. The latter governs the amount of soil non-linearity mobilized and the resulting local stiffness, in turn affecting the requirements for accurate constitutive integration.

In Figure 21, the parametric study in Figures 16-17 is replicated for a higher input amplitude ($A = 1$ mm) and the same two different h values (cases VMKH6-7 in Table 2). **The time domain plots provided testify the effects of grid spacing on the predicted response: again, they mostly concern the final residual displacement, more pronouncedly as** h **decreases. The same previous uncertainties about the interplay of grid spacing effects and constitutive integration still apply to this case.**

The discussion on the influence of Δt at higher input amplitude refers to Figures 22–23, illustrating the results obtained for $\Delta x = \Delta x_{std}$ and h equal to $0.5E$, $0.05E$ and $0.01E$ (cases VMKH8-10 in Table 2); **again, EM/PM plots comes from the numerical reference solution corresponding with** $\Delta t = \Delta t_{std}/5 =$ **0.0001 s.**

The comparison of Figures 21 and 22 suggests that, even with a much larger input amplitude, $\Delta x = \Delta x_{std}$ is still an appropriate grid spacing for elastic-plastic problems, as long as Δt is substantially reduced to comply with (explicit) constitutive integration requirements. **This inference is supported by the following observations:**

- Δt **affects not only the residual component of displacement time histories (as in Figure 21), but also their maximum/minimum transient values – i.e. the numerical representation of plastic dissipation. This is clearly visible in Figure 22(a);**
- **EM/PM values are in general higher at larger input amplitude (Figure 22(d)), and experience a slower decrease as** Δt **is reduced (still depending on the specific** h **value);**

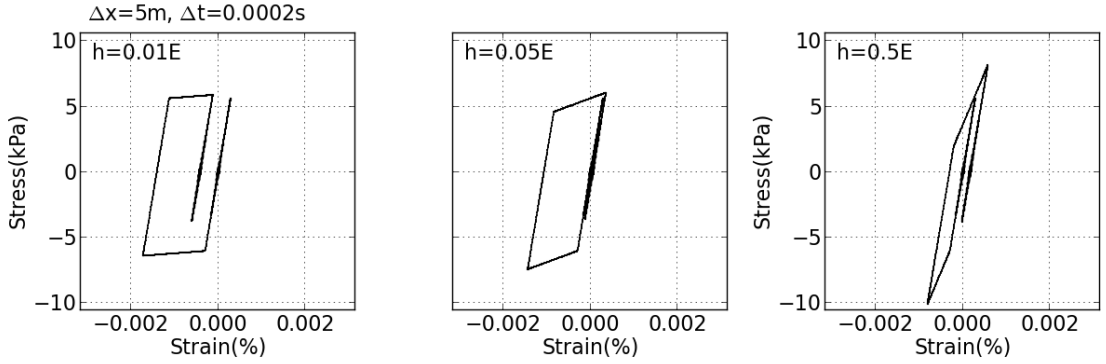

(a) Δt=0.0002 s

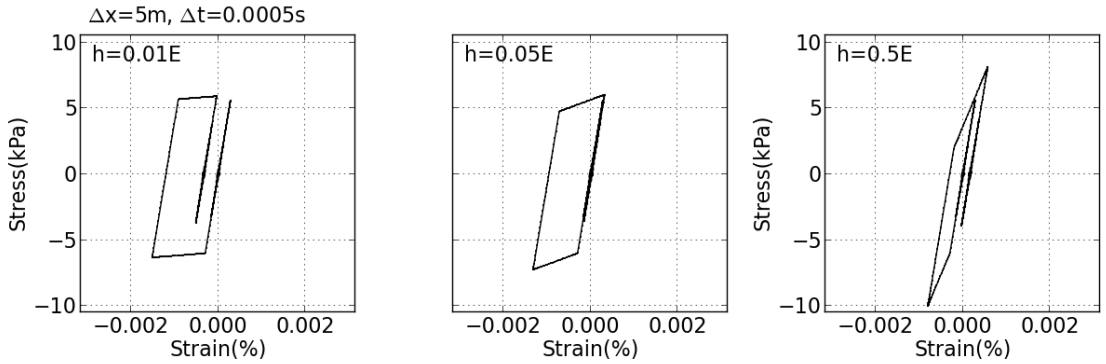

(b) Δt=0.0005 s

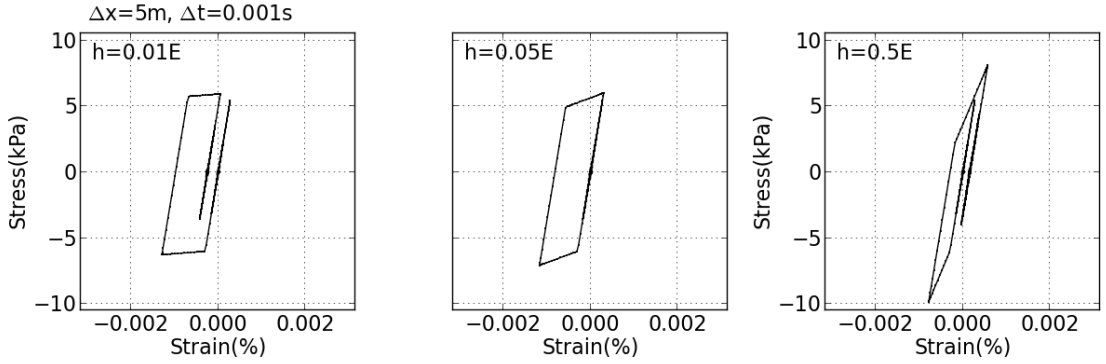

(c) Δt=0.001 s

Figure 20: Influence of time-step size, shear stress-strain response at the bottom of the VMKH sub-layer, cases VMKH3 ($h = 0.5E$), VMKH4 ($h = 0.05E$) and VMKH5 ($h = 0.01E$), ($\Delta x_{std} =$ 5 m, $\Delta t_{std} = 0.0005$ s, $\Delta x = 5$ m, $A = 0.1$ mm)

- **the shear stress-strain loops in Figure 23 show how inaccurate the simulated constitutive response can be when Δt is too large (e.g. Δ = 0.001 s) and substantial plastic degradation of material stiffness takes place (see the case $h = 0.01E$).**

This set of results suggests that Δt should be at least in the order of $\Delta x/20V_s$ for acceptable constitutive integration and overall accuracy in elastic-plastic wave simulations. However, such a conclusion seems quite heuristic, as it may be altered by the use of different material models (see next section) and stress-point algorithms.

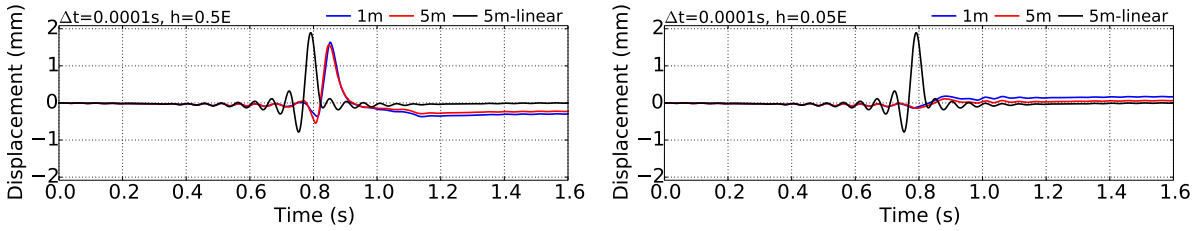

(a) Displacement time history, $h = 0.5E$ (2.2–3.8 s) (b) Displacement time history, $h = 0.05E$ (2.2–3.8 s)

Figure 21: Influence of grid spacing, displacement plot, cases VMKH6 ($h = 0.5E$) and VMKH7 ($h = 0.05E$) ($\Delta x_{std} = 5$ m, $\Delta t_{std} = 0.0005$ s, Δx =1, 5 m, $\Delta t = 0.0001$s, $A = 1$ mm)

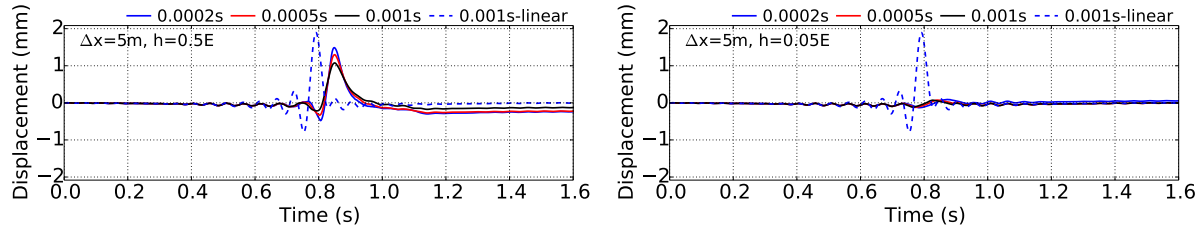

(a) Displacement time history, $h = 0.5E$ (2.2–3.8 s) (b) Displacement time history, $h = 0.05E$ (2.2–3.8 s)

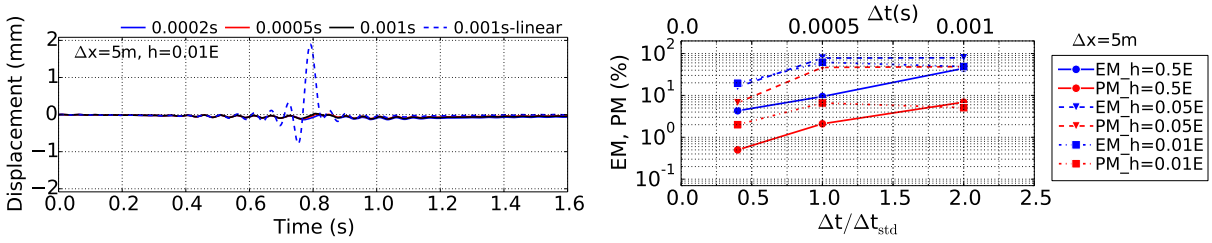

(c) Displacement time history, $h = 0.01E$ (2.2–3.8 s) (d) EM/PM misfits (ref. solution: $\Delta t = 0.0001$ s)

Figure 22: Influence of time-step size, displacement plot, cases VMKH8 ($h = 0.5E$), VMKH9 ($h = 0.05E$) and VMKH10 ($h = 0.01E$) ($\Delta x_{std} = 5$ m, $\Delta t_{std} = 0.0005$ s, $\Delta x = 5$ m, $\Delta t =$ 0.0002, 0.0005, 0.001 s, $A = 1$ mm)

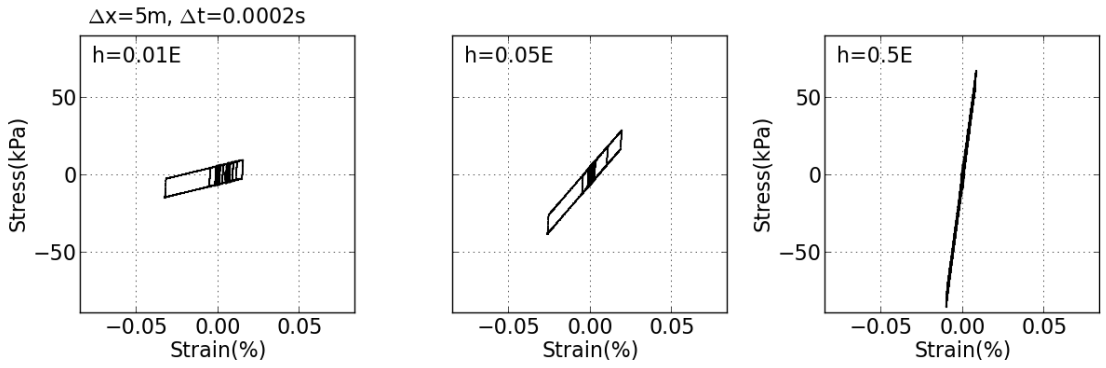

(a) Δt=0.0002 s

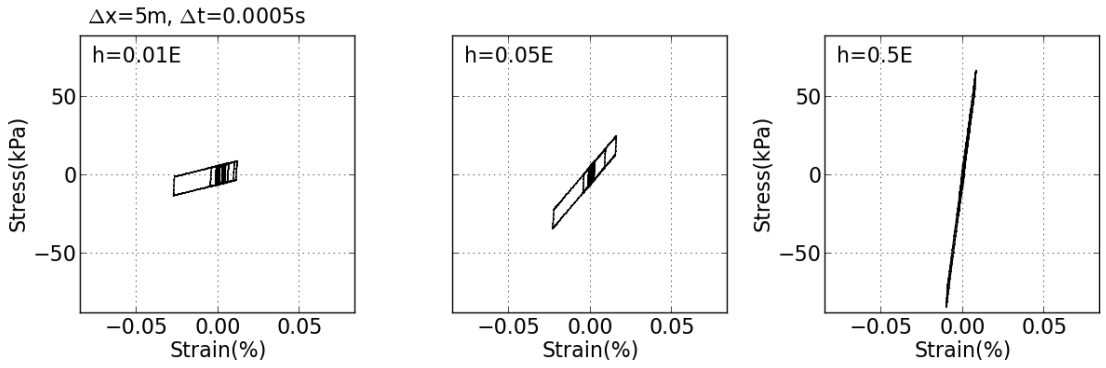

(b) Δt=0.0005 s

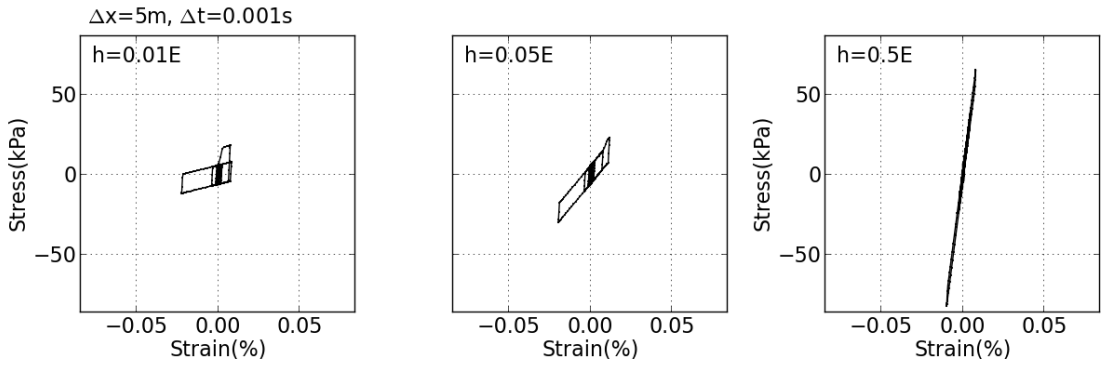

(c) Δt=0.001 s

Figure 23: Influence of time-step size, shear stress-strain response at the bottom of the VMKH sub-layer, cases VMKH8 ($h = 0.5E$), VMKH9 ($h = 0.05E$) and VMKH10 ($h = 0.01E$) ($\Delta x_{std} = 5$ m, $\Delta t_{std} = 0.0005$ s, $\Delta x = 5$ m, $A = 1$ mm)

4.2 PBS model

4.2.1 Model parameters and parametric analysis

The influence of space/time discretization is now explored in combination with the non-linear PBS soil model introduced in Section 2.2.3 (Pisanò and Jeremić, 2014). As in real geomaterials, the PBS model features an elastic-plastic response since the very onset of loading (vanishing yield locus), with the stiffness smoothly evolving from small-strain elastic behavior to failure (nil stiffness).

The results presented hereafter concern a 500 m thick soil layer, whose upper 100 m are made of a non-linear PBS soil resting on a 400 m elastic sub-layer. As done for the VMKH simulations, a thin layer (2.5 m) of elastic material has been added to prevent numerical problems with very strong motions and the whip effect at the ground surface. Input 1 with $A = 1$ mm has been exclusively considered, along with the following set of PBS parameters (Pisanò and Jeremić, 2014) (same elastic parameters for both the PBS and the elastic sub-layers):

- $\rho = 2000$ kg/m^3, $E = 1.3$ GPa and $\nu = 0.3$, implying an elastic shear wave velocity $V_s = 500$ m/s ;
- shear strength parameter: $M = 1.2$, corresponding with friction angle equal to 30 deg under triaxial compression;
- dilatancy parameters: $k_d = 0.0$ and $\xi = 0.0$[5];
- hardening parameters: $h = 300$ and $m = 1$.

The list of PBS simulations is reported in Table 3, while the next figures will also point out the good performance of the PBS model in reproducing the cyclic soil behavior.

case #	Δx_{std} [m]	Δt_{std} [s]	Δx [m]	Δt [s]	A [mm]
PBS1	2.5	0.0005	0.5, 2.5	0.0001	1
PBS2	2.5	0.0005	0.1, 0.5, 1	0.00002	1
PBS3	2.5	0.0005	2.5	0.0002, 0.0005, 0.001	1
PBS4	2.5	0.0005	2.5	0.00001, 0.00002, 0.0001	1

Table 3: List of PBS simulations

[5]Soil volume changes under shear loading have been inhibited for the sake of simplicity. This aspect would further affect the overall stiffness of the soil layer and require additional parametric analyses.

4.2.2 Influence of grid spacing and time-step size

Most of the issues observed in VMKH simulations appear to be magnified by the more complex PBS model. A summary of the main inferences drawn on the basis of Figures 24–30 is provided here below:

- grid spacing turns out to be influential again (Figures 24 and 26), as a consequence of more severe variations (than in VMKH cases) in shear stiffness during cyclic loading. In fact, one would have to follow the stiffness reduction curves arising from the constitutive response, and use minimum stiffness to decide on space discretization;
- **as in VMKH simulations, grid spacing mainly affects residual displacements. This is clearly shown by the EM/PM plots in Figure 26(b), where EM errors larger than 10% arise even for a very small time-step size ($\Delta t = \Delta t_{std}/25 =$ 0.00002 s); conversely, phase misfits are less affected by residual displacements and thus always quite limited. In presence of high non-linearity, it seems safer to use Δx $4 \div 5$ times smaller than $\Delta x_{std} = V/10 f_{max}$;**
- **the combination of explicit constitutive integration and high non-linearity makes time-stepping effects quite prominent, as is shown by Figures 27 and 28. Further, Figures 29 leads to conclude that $\Delta t = \Delta t_{std}/50$ may be needed to obtain EM errors lower than 10% (Figures 29-30). Apparently, analysts have to compromise on accuracy and computational costs in these situations;**
- as expected, the shear stress-strain cycles in Figures 25 and 28 show that the sensitivity to discretization builds up as increasing non-linearity is mobilized. **This is the case for instance at the top of the PBS layer, where cycles are more dissipative than at the bottom due to lower overburden stresses and dynamic amplification.**

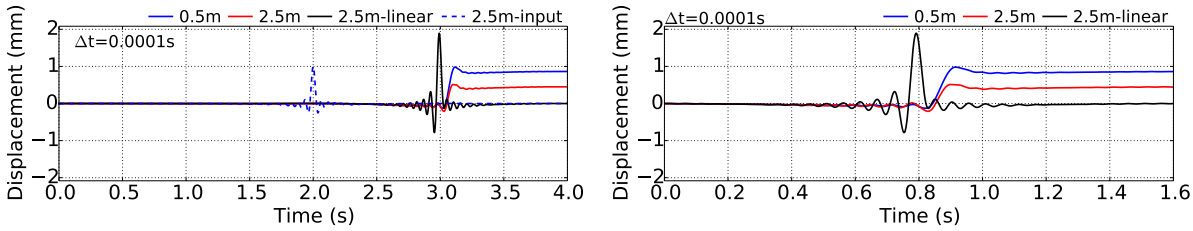

(a) Displacement time history (0.0–4.0 s)

(b) Displacement time history (2.2–3.8 s)

Figure 24: Influence of grid spacing, displacement plot, case PBS1 ($\Delta x_{std} =$ 2.5 m, $\Delta t_{std} =$ 0.0005 s, $\Delta x =$ 0.5, 2.5 m, $\Delta t =$ 0.0001 s, $A =$ 1 mm)

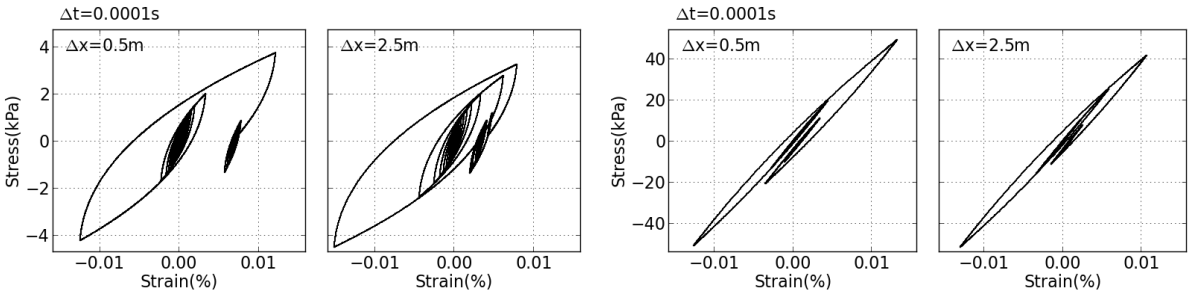

(a) At the top of the layer

(b) At the bottom of the layer

Figure 25: Influence of grid spacing, shear stress-strain response in the PBS sub-layer, case PBS1 (Δx_{std} = 2.5 m, Δt_{std} = 0.0005 s, Δx = 0.5, 2.5 m, Δt = 0.0001 s, A = 1 mm)

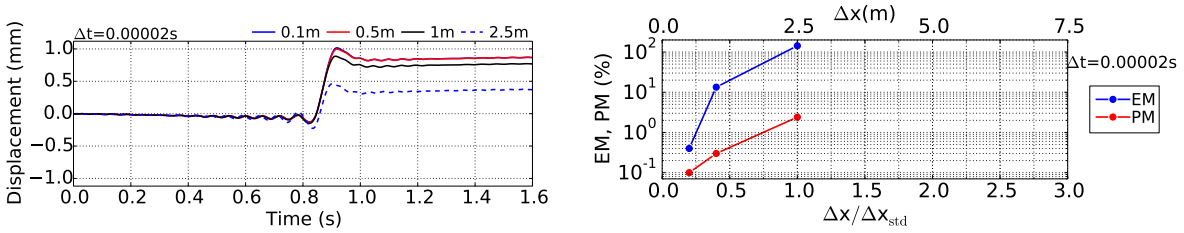

(a) Displacement time history (2.2–3.8 s)

(b) EM/PM misfits (ref. solution: Δx = m **KOHEI?**)

Figure 26: Influence of grid spacing, displacement plot, case PBS2 (Δx_{std} = 2.5 m, Δt_{std} = 0.0005 s, Δx = 0.1, 0.5, 1 m, Δt = 0.00002 s, A = 1 mm)

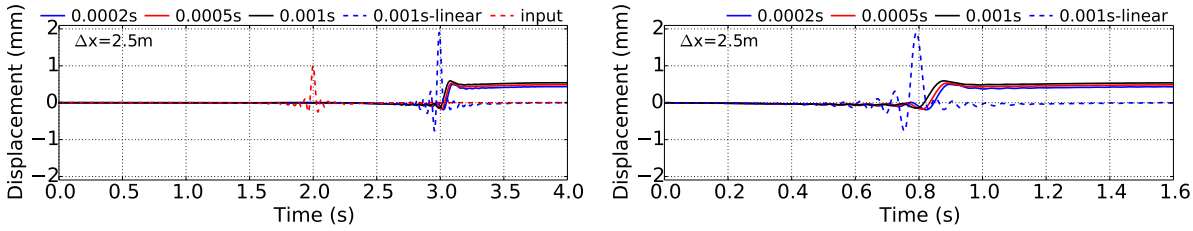

(a) Displacement time history (0.0–4.0 s)

(b) Displacement time history (2.2–3.8 s)

Figure 27: Influence of time-step size, displacement plot, case PBS3 (Δx_{std} = 2.5 m, Δt_{std} = 0.0005 s, Δx = 2.5 m, Δt = 0.0002, 0.0005, 0.001 s, A = 1 mm)

Since displacement components result from strains through spatial integration, the displacement performance can be well-predicted on condition that strains are accurately computed all along the soil domain. For the same reason, the discretization requirements for displacement convergence are not uniform along the soil deposit. Figures 31 and 32 illustrate in the time domain the displacements simulated at different depths in the non-linear sub-layer (the vertical x axis points upward – Figure 1) and at different Δx and Δt. These figures clearly point out that accuracy requirements may be more or less hard to satisfy depending on the specific spatial

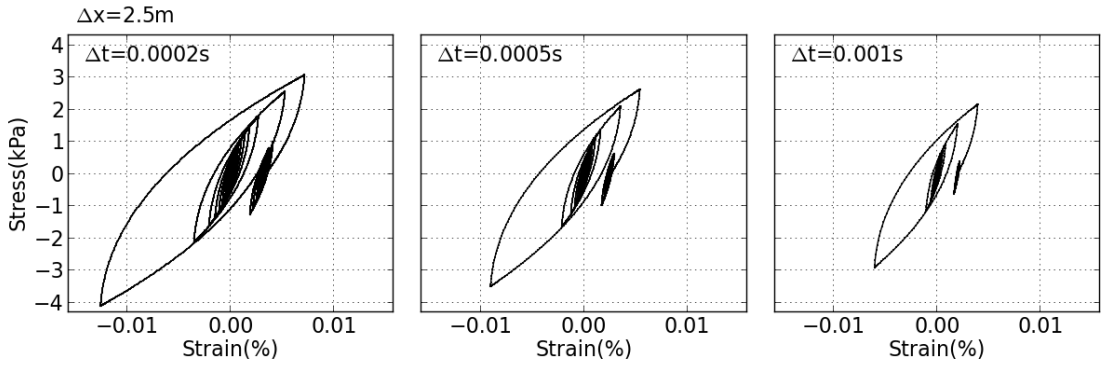

(a) At the top of the layer

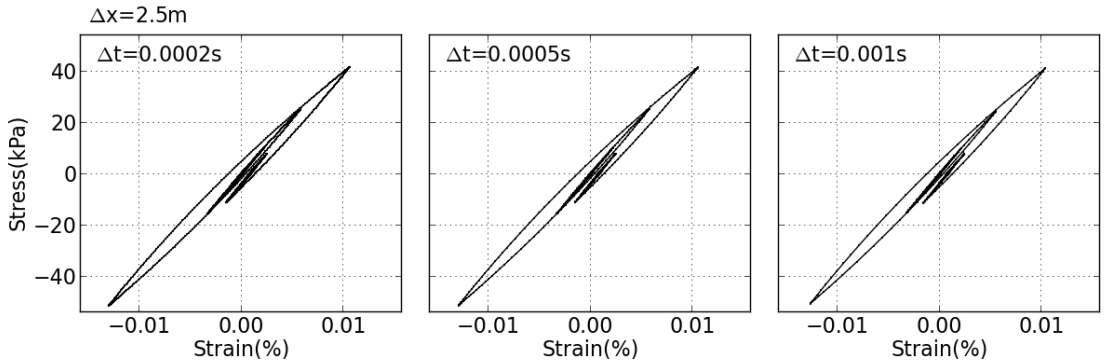

(b) At the bottom of the layer

Figure 28: Influence of time-step size, shear stress-strain response in the PBS sub-layer, case PBS3 (Δx_{std} = 2.5 m, Δt_{std} = 0.0005 s, Δx = 2.5 m, Δt = 0.0002, 0.0005, 0.001 s, A = 1 mm)

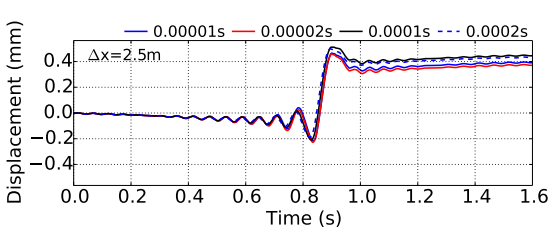

(a) Displacement time history (2.2–3.8 s)

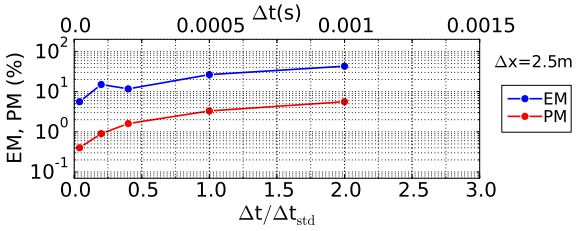

(b) EM/PM misfits (ref. solution: Δt = s **KOHEI?**)

Figure 29: Influence of time-step size, displacement plot, case PBS4 (Δx_{std} = 2.5. m, Δt_{std} = 0.0005 s, Δx = 2.5 m, Δt = 0.00001, 0.00002,0.0001 s, A = 1 mm)

location. In 1D wave propagation problems, faster convergence is attained far from the ground surface, since this implies satisfactory accuracy in a lower number of nodes and integration points.

Conversely, the close relationship between plastic strains and residual displacements has slender influence on acceleration components. In this respect, Figures 33 and

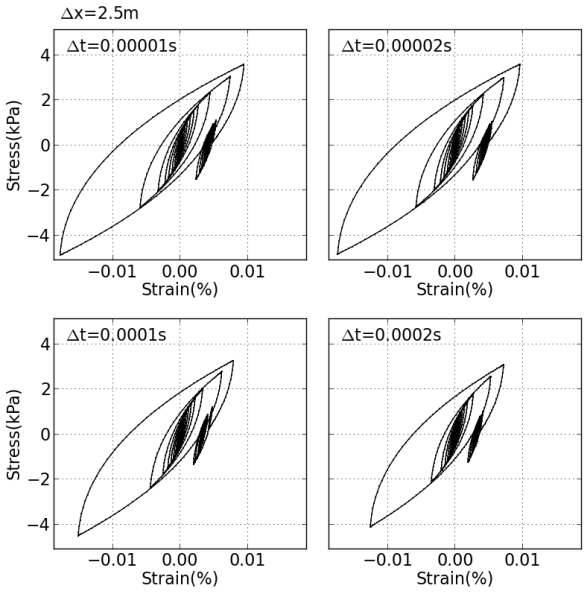

Figure 30: Influence of time-step size, shear stress-strain response at the bottom of the PBS sub-layer, case PBS4 ($\Delta x_{std} = 2.5$ m, $\Delta t_{std} = 0.0005$ s, $\Delta x = 2.5$ m, $\Delta t = 0.00001$, 0.00002,0.0001 s, $A = 1$ mm)

34 show that, as long as reasonable grid spacing is set (perhaps in the order of $\Delta x_{std}/2 = V_s/20 f_{max}$), the sensitivity of acceleration components to Δt is practically negligible (or definitely weaker than for residual displacements).

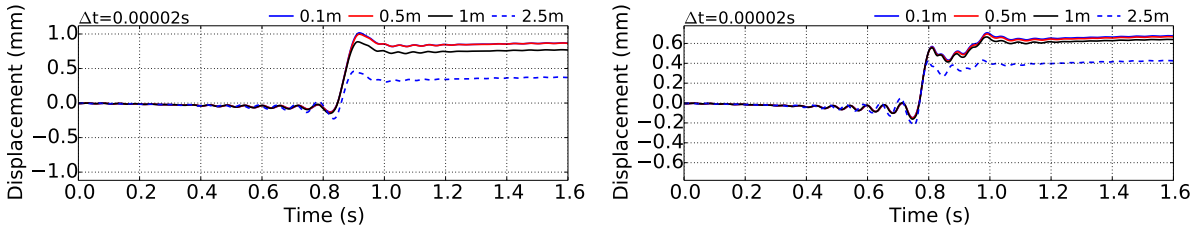

(a) x=500 m

(b) x=480m

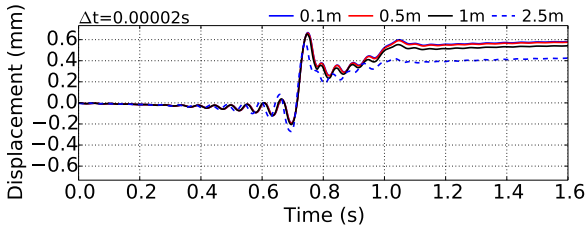

(c) x=460 m

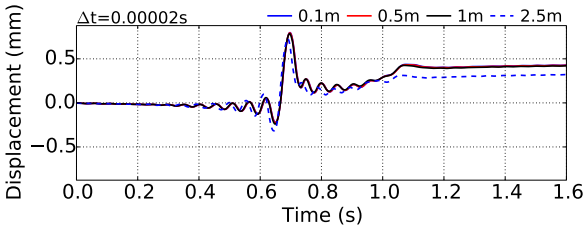

(d) x=440 m

Figure 31: Influence of grid spacing at different locations along the PBS layer, displacement plot, PBS2 case (Δx_{std} = 2.5 m, Δt_{std} = 0.0005 s, Δx = 0.1, 0.5, 1 m, Δt = 0.00002 s, A = 1 mm)

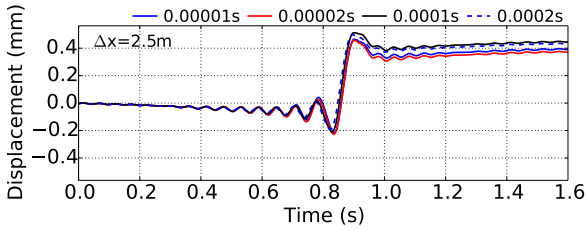

(a) x=500 m

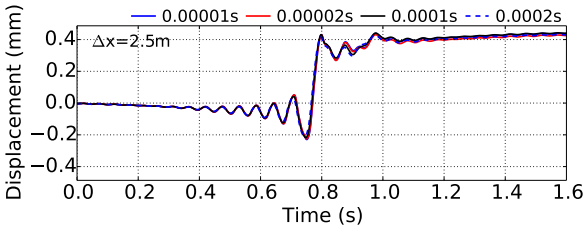

(b) x=480 m

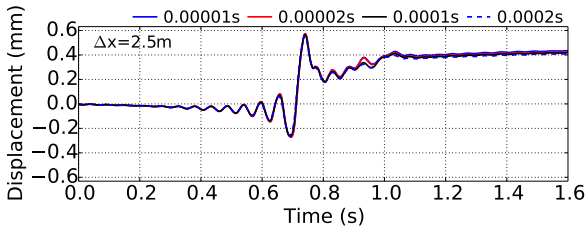

(c) x=460 m

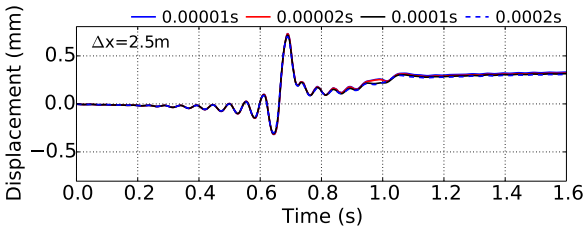

(d) x=440 m

Figure 32: Influence of time-step size at different locations along the PBS layer, displacement plot, PBS4 case (Δx_{std} = 2.5. m, Δt_{std} = 0.0005 s, Δx = 2.5 m, Δt = 0.00001, 0.00002, 0.0001 s, A = 1 mm)

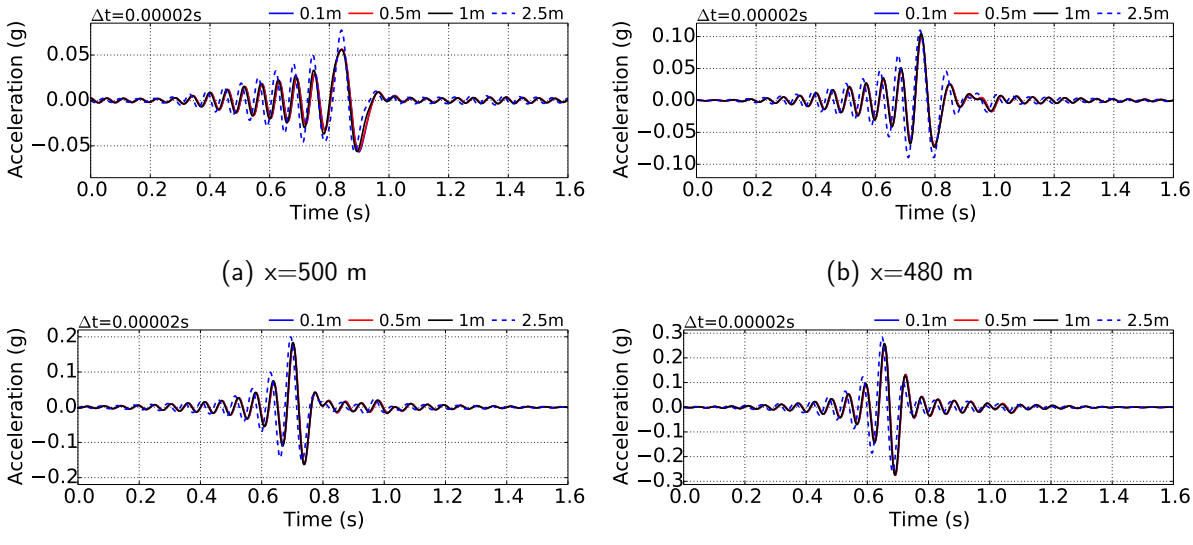

(a) x=500 m

(b) x=480 m

(c) x=460 m

(d) x=440 m

Figure 33: Influence of grid spacing at different locations along the PBS layer, acceleration plot, PBS2 case (Δx_{std} = 2.5 m, Δt_{std} = 0.0005 s, Δx = 0.1, 0.5, 1 m, Δt = 0.00002 s, A = 1 mm)

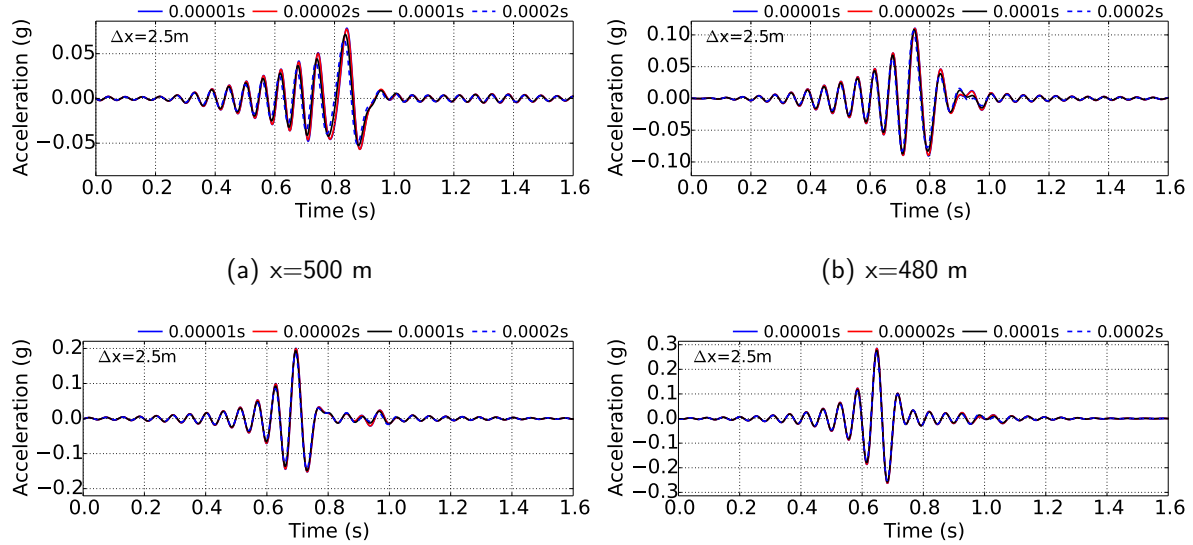

(a) x=500 m

(b) x=480 m

(c) x=460 m

(d) x=440 m

Figure 34: Influence of time-step size at different locations along the PBS layer, acceleration plot, PBS4 case (Δx_{std} = 2.5 m, Δt_{std} = 0.0005 s, Δx = 2.5 m, Δt = 0.00001, 0.00002, 0.0001 s, A = 1 mm)

5 Concluding remarks

Previously established criteria for space/time discretization in wave propagation FE simulations have been re-appraised and critically discussed, in order to provide more solid ground to verification procedures in Computational Dynamics. The 1D propagation of seismic shear waves (Ormsby wavelets) through both linear and non-linear (elastic-plastic) media has been numerically simulated, with focus on capturing high-frequency motion and exploring the relationship between material response and discretization requirements. After initial linear computations, two different material models (referred to as VMKH and PBS) have been used at increasing level of complexity. The main conclusions inferred are hereafter summarized:

Elastic simulations Setting grid spacing and time-step size as per standard rules ($\Delta x_{std} = V_s/10f_{max}$ and $\Delta t_{std} = \Delta t/V_s$) has proven not to be always appropriate, especially to reproduce high-frequency motion components (this can be clearly visualized in the Fourier phase plane). When linear elements (8-node bricks) are used, $\Delta x \approx \Delta x_{std}/2$ and $\Delta t \approx \Delta t_{std}/2$ seem to ensure sufficient accuracy over the whole frequency range (both in amplitude and phase); higher order elements (e.g. 27-node bricks), will allow the use of $\Delta x = \Delta x_{std}$ still in combination with $\Delta t \approx \Delta t_{std}/2$. Preserving accuracy in simulations including large domains and/or time intervals seems intrinsically more difficult, since attenuation/dispersion phenomena are cumulative.

Elastic-plastic simulations Conclusive criteria for elastic-plastic problems can be hardly established, as space/time discretization also interferes with the integration of non-linear constitutive equations. In this respect, different outcomes may be found depending on (i) the kind and amount of non-linearity associated with the material model (stiffness variations during straining), (ii) stress-point integration algorithm (e.g. explicit or implicit), (iii) the amplitude of the input motion, affecting the amount of material plasticity mobilized during wave motion. The experience gained through the use of the PBS model (explicitly integrated in 8-node brick elements) suggests that $\Delta x_{std} = V_s/10f_{max}$ and $\Delta t_{std} = \Delta t/10V_s$ may need to be reduced by factors up to $4 \div 5$ and 500, respectively, in the presence of strong input motions and severe stiffness variations. Importantly, these conclusions also depend on what output component is being considered and where within the computational domain.

It is also worth remarking that the present study may not be regarded as conclusive, especially when it comes to non-linear wave problems. There are in fact several aspects that will deserve in the future further consideration, such as the implications of using higher-order finite elements. The same comment also applies to geometrical effects (e.g. scattering) in 2D/3D problems, whose influence on discretization criteria for elastic-plastic simulations would be per se a whole research topic.

In the authors' hope, this study will reopen the discussion on a subject that is as relevant as often overlooked. Nowadays, modern computational platforms are increasingly supporting engineering analysis and decision-making, that should always be supported by robust verification procedures. As shown for non-linear wave problems, combining knowledge in computational methods and material mechanics seems to be the way towards more reliable numerical simulations.

6 Acknowledgements

The Authors wish to acknowledge the financial support from the US-NRC, US-DOE and Shimizu Inc. Corporation (Japan).

References

J. H. Argyris and H.-P. Mlejnek. *Dynamics of structures*. North-Holland Amsterdam, 1991.

I. Babuska and J. T. Oden. Verification and validation in computational engineering and science: basic concepts. *Computer Methods in Applied Mechanics and Engineering*, 193(36):4057–4066, 2004.

H. Bao, J. Bielak, O. Ghattas, L. F. Kallivokas, D. R. O'Hallaron, J. R. Shewchuk, and J. Xu. Large-scale simulation of elastic wave propagation in heterogeneous media on parallel computers. *Computer Methods in Applied Mechanics and Engineering*, 152(1-2):85–102, January 1998.

A. Bayliss, C. I. Goldstein, and E. Turkel. On accuracy conditions for the numerical computation of waves. *Journal of Computational Physics*, 59(3):396–404, 1985.

M. Benjemaa, N. Glinsky-Olivier, V. Cruz-Atienza, J. Virieux, and S. Piperno. Dynamic non-planar crack rupture by a finite volume method. *Geophysical Journal International*, 171(1):271–285, 2007.

J. Bielak, K. Loukakis, Y. Hisada, and C. Yoshimura. Domain reduction method for three–dimensional earthquake modeling in localized regions. part I: Theory. *Bulletin of the Seismological Society of America*, 93(2):817–824, 2003.

R. I. Borja. *Plasticity Modeling & Computation*. Springer-Verlag, 2013.

R. I. Borja and A. P. Amies. Multiaxial cyclic plasticity model for clays. *Journal of geotechnical engineering*, 120(6):1051–1070, 1994.

R. I. Borja, H.-Y. Chao, F. J. Montáns, and C.-H. Lin. Nonlinear ground response at lotung lsst site. *Journal of geotechnical and geoenvironmental engineering*, 125(3):187–197, 1999.

W. F. Chen and D. J. Han. *Plasticity for Structural Engineers*. Springer Verlag, 1988.

Z. Cheng and B. Jeremić. Numerical modeling and simulation of pile in liquefiable soil. *Soil Dynamics and Earthquake Engineering*, 29(11):1405–1416, 2009.

A. K. Chopra. *Dynamics of structures: theory and applications to earthquake engineering*. Prentice Hall (2nd edition), 2000.

J. D. De Basabe and M. K. Sen. Grid dispersion and stability criteria of some common finite-element methods for acoustic and elastic wave equations. *Geophysics*, 72(6):T81–T95, 2007.

C. S. Desai and H. J. Siriwardane. *Constitutive Laws for Engineering Materials With Emphasis on Geologic Materials*. Prentice–Hall, Inc. Englewood Cliffs, NJ 07632, 1984.

C. di Prisco and F. Pisanò. Seismic response of rigid shallow footings. *European Journal of Environmental and Civil Engineering*, 15(sup1):185–221, 2011.

C. di Prisco, M. Pastor, and F. Pisanò. Shear wave propagation along infinite slopes: A theoretically based numerical study. *International Journal for Numerical and Analytical Methods in Geomechanics*, 36(5):619–642, 2012.

C. G. di Prisco and D. M. Wood. *Mechanical behaviour of soils under environmentallly-induced cyclic loads*, volume 534. Springer, 2012.

A. Fichtner and H. Igel. Efficient numerical surface wave propagation through the optimization of discrete crustal modelsa technique based on non-linear dispersion curve matching (DCM). *Geophysical Journal International*, 173(2):519–533, 2008.

G. Gazetas and G. Mylonakis. Seismic soil-structure interaction: new evidence and emerging issues. In *Geotechnical earthquake engineering and soil dynamics III*, pages 1119–1174. ASCE, 1998.

K. F. Graff. *Wave motion in elastic solids*. Courier Dover Publications, 1975.

M. Holschneider. *Wavelets: an analysis tool*. Oxford Science Publications, Oxford, UK, 1995.

T. J. Hughes. *The finite element method: linear static and dynamic finite element analysis*. Courier Dover Publications, 2012.

K. Ishihara. Soil behaviour in earthquake geotechnics. 1996.

B. Jeremić and G. Jie. Parallel soil–foundation–structure computations. In N. L. M. Papadrakakis, D.C. Charmpis and Y. Tsompanakis, editors, *Progress in Computational Dynamics and Earthquake Engineering*. Taylor and Francis Publishers, 2008.

B. Jeremić, Z. Yang, Z. Cheng, G. Jie, K. Sett, M. Taiebat, M. Preisig, N. Tafazzoli, P. Tasiopoulou, J. A. A. Mena, F. Pisanò, K. Watanabe, and K. Karapiperis. Lecture notes on computational geomechanics: Inelastic finite elements for pressure sensitive materials. Technical Report UCD-CompGeoMech–01–2004, University of California, Davis, 1989-2015.

B. Jeremić, Z. Cheng, M. Taiebat, and Y. Dafalias. Numerical simulation of fully saturated porous materials. *International Journal for Numerical and Analytical Methods in Geomechanics*, 32(13): 1635–1660, 2008.

B. Jeremić, G. Jie, M. Preisig, and N. Tafazzoli. Time domain simulation of soil–foundation–structure interaction in non-uniform soils. *Earthquake Engineering and Structural Dynamics*, 38(5):699–718, 2009.

B. Jeremić, R. Roche-Rivera, A. Kammerer, J. Tafazzoli, Nima Abell, B. Kamranimoghaddam, F. Pisanò, C. Jeong, and B. Aldridge. The nrc essi simulator program: current status. In *Proceedings of the Structural Mechanics in Reactor Technology (SMiRT) 2013 Conference (San Francisco, August 18-23, 2013)*, 2013a.

B. Jeremić, N. Tafazzoli, T. Ancheta, N. Orbović, and A. Blahoianu. Seismic behavior of npp structures subjected to realistic 3d, inclined seismic motions, in variable layered soil/rock, on surface or embedded foundations. *Nuclear Engineering and Design*, 265:85–94, 2013b.

M. Kaser, V. Hermann, and J. de la Puente. Quantitative accuracy analysis of the discontinuous galerkin method for seismic wave propagation. *Geophysical Journal International*, 173:990–999, 2008.

E. Kausel. *Fundamental solutions in elastodynamics: a compendium*. Cambridge University Press, 2006.

E. Kausel and G. Manolis. *Wave motion in earthquake engineering*. Wit Press, 2000.

H. Kolsky. *Stress waves in solids*, volume 1098. Courier Dover Publications, 1963.

S. Kramer. Geotechnical earthquake engineering. *New Jersey*, 1996.

M. Kristekova, J. Kristek, P. Moczo, and D. S. M. Misfit criteria for quantitative comparison of seismograms. *Bullettin of the Seismological Society of America*, 96(5):1836–1850, 2006.

M. Kristekova, J. Kristek, and M. P. Time-frequency misfit and goodness-of-fit criteria for quantitative comparison of time signals. *Geophysical Journal International*, 178:813–825, 2009.

R. Kuhlemeyer and J. Lysmer. Finite element method accuracy for wave propagation problems. *Journal of Soil Mechanics & Foundations Division*, 99(Tech Rpt), 1973.

C. G. Lai and K. Wilmanski. *Surface waves in geomechanics: Direct and inverse modelling for soils and rocks*, volume 481. Springer, 2005.

J. Lemaitre and J. L. Chaboche. *Mechanics of solid materials*. Cambridge university press, 1990.

J. Lysmer and R. Kuhlemeyer. Finite dynamic model for infinite media. *ASCE Journal of Engineering Mechanics Division*, 95(EM4):859–877, 1969.

P. Moczo, J. Kristek, M. Galis, P. Pazak, and M. Balazovjech. The finite-difference and finite-element modeling of seismic wave propagation and earthquake motion. *Acta physica slovaca*, 57(2), 2007.

N. M. Newmark. A method of computation for structural dynamics. *Journal of the Engineering Mechanics Division*, 85(3):67–94, 1959.

R. Nova. *Soil mechanics*. John Wiley & Sons, 2012.

W. L. Oberkampf, T. G. Trucano, and C. Hirsch. Verification, validation, and predictive capability in computational engineering and physics. *Applied Mechanics Reviews*, 57(5):345–384, 2004.

N. Orbović, B. Jeremić, J. Abell, C. Luo, R. P. Kennedy, and A. Blaihoanu. Use of non-linear, time domain analysis for design. In *Proceedings of the Structural Mechanics in Reactor Technology (SMiRT) 2015 Conference (Manchester, August 10-14, 2015)*, 2015.

J. Pérez-Ruiz, F. Luzón, and A. García-Jerez. Scattering of elastic waves in cracked media using a finite difference method. *Studia Geophysica et Geodaetica*, 51(1):59–88, 2007.

F. Pisanò and B. Jeremić. Simulating stiffness degradation and damping in soils via a simple visco-elastic–plastic model. *Soil Dynamics and Earthquake Engineering*, 63:98–109, 2014.

J. H. Prevost. *DYNA1D: A Computer Program for Nonlinear Seismic Site Response Analysis Technical Documentation*. National Center for Earthquake Engineering Research, 1989.

A. Quarteroni and A. Valli. *Numerical approximation of partial differential equations*, volume 23. Springer, 2008.

M. Randolph and M. R. S. Gourvenec. *Offshore geotechnical engineering*. CRC Press, 2011.

C. J. Roy and W. L. Oberkampf. A comprehensive framework for verification, validation, and uncertainty quantification in scientific computing. *Computer Methods in Applied Mechanics and Engineering*, 200(25):2131–2144, 2011.

H. Ryan. Ricker, Ormsby, Klauder, Butterworth - a choice of wavelets. *Canadian Society of Exploration Geophysicists*, 19(7):8–9, 1994.

J. F. Semblat and A. Pecker. *Waves and vibrations in soils: earthquakes, traffic, shocks, construction works*. IUSS Press, 2009.

J. Simo and T. Hughes. *Computational Inelasticity*, volume 7. Springer, 1998.

W. D. Smith. The application of finite element analysis to body wave propagation problems. *Geophysical Journal International*, 42(2):747–768, 1975.

M. Taiebat, B. Jeremić, Y. F. Dafalias, A. M. Kaynia, and Z. Cheng. Propagation of seismic waves through liquefied soils. *Soil Dynamics and Earthquake Engineering*, 30(4):236–257, 2010.

P. Tasiopoulou, M. Taiebat, N. Tafazzoli, and B. Jeremić. On validation of fully coupled behavior of porous media using centrifuge test results. 2015a.

P. Tasiopoulou, M. Taiebat, N. Tafazzoli, and B. Jeremic. Solution verification procedures for modeling and simulation of fully coupled porous media: static and dynamic behavior. *Coupled Systems Mechanics Journal*, 4(1):67–98, 2015b.

J. P. Wolf. *Dynamic soil-structure interaction*. Englewood Cliffs, 1985.

D. Wood. *Geotechnical modelling*. Spon Press, 2004.

C. Yoshimura, J. Bielak, and Y. Hisada. Domain reduction method for three–dimensional earthquake modeling in localized regions. part II: Verification and examples. *Bulletin of the Seismological Society of America*, 93(2):825–840, 2003.

O. Zienkiewicz and R. Taylor. *The finite element method. Vol. 1: Its basis and fundamentals (5th edition)*. Butterworth-Heinemann, 2000.

O. C. Zienkiewicz, A. Chan, M. Pastor, B. Schrefler, and T. Shiomi. *Computational geomechanics – with special reference to earthquake engineering*. Wiley Chichester, 1999.